Unusual Metal-Organic Multicomponent Ni(II) and Mononuclear Zn(II) Compounds Involving Pyridine Dicarboxylates: Supamolecular Assemblies and Theoretical Studies

Kamal K. Dutta , Pranay Sharma , Subham Banik , Rosa M. Gomila , Antonio Frontera * , Miquel Barceló-Oliver , Manjit K. Bhattacharyya *

Posted Date: 15 August 2024

doi: 10.20944/preprints202408.1099.v1

Keywords: multicomponent Ni(II); dual enclathration; C–H···π(chelate ring); DFT; combined QTAIM/NCI plot analysis

 doi:10.20944/preprints202408.1099.v1

Article

Unusual Metal-Organic Multicomponent Ni(II) and Mononuclear Zn(II) Compounds Involving Pyridine Dicarboxylates: Supamolecular Assemblies and Theoretical Studies

Kamal K. Dutta [1], Pranay Sharma [1], Subham Banik [1], Rosa M. Gomila [2], Antonio Frontera [2,*], Miquel Barcelo-Oliver [2] and Manjit K. Bhattacharyya [1,*]

[1] Department of Chemistry, Cotton University, Guwahati-781001, Assam, India
[2] Departament de Química, Universitat de les Illes Balears, Crta de Valldemossa km 7.7, 07122 Palma de Mallorca (Baleares), Spain
* Correspondence: toni.frontera@uib.es (A.F.); manjit.bhattacharyya@cottonuniversity.ac.in (M.K.B.)

Abstract: Herein, we have reported the synthesis and characterization [single crystal X-ray diffraction technique, spectroscopic etc.] of two new Ni(II) and Zn(II) coordination compounds *viz.* $[Ni(2,6\text{-}PDC)_2]_2[Ni(en)_2(H_2O)_2]_2[Ni(en)(H_2O)_4]\cdot 4H_2O$ (**1**) and $[Zn(2,6\text{-}PDC)(Hdmpz)_2]$ (**2**) (where, 2,6-PDC = 2,6-pyridinedicarboxylate, en = ethylene-1,2-diamine, Hdmpz = 3,5-dimethyl pyrazole). Compound **1** is found to crystallize as a multicomponent Ni(II) compound with five discrete complex moieties; whereas, compound **2** is a mononuclear compound of Zn(II). Deep analysis of the crystal structure of compound **1** unfolds unusual dual enclathration of guest complex cationic moieties within the supramolecular host cavity stabilized by anion–π, π-stacking, N–H···O, C–H···O and O–H···O hydrogen bonding interactions. Interestingly, further enclathration of a complex cationic moiety is observed within another supramolecular host cavity formed involving anionic complex moieties and lattice water molecules in **1**. Again, the crystal structure of compound **2** is stabilized by the presence of unconventional C–H···π(chelate ring) interactions along with C–H···O, C–H···N hydrogen bonding, π-stacking, C–H···π(pyridyl) interactions. These non-covalent interactions have been further studied theoretically using density functional theory (DFT) calculations, molecular electrostatic potential (MEP) surfaces, non-covalent interaction (NCI) plot index and quantum theory of atoms in molecules (QTAIM) computational tools. The computational study displays that π-stacking or H-bonds greatly tune the directionality of compound **1** although non-directional electrostatic forces dominate energetically. For compound **2**, combined QTAIM/NCI plot analysis confirms the presence of unconventional C–H···π(chelate ring) interaction along with other weak interactions obtained from the crystal structure analysis. Further, the individual energy contributions of these weak yet significant non-covalent interactions have also been determined computationally.

Keywords: multicomponent Ni(II); dual enclathration; C–H···π(chelate ring); DFT; combined QTAIM/NCI plot analysis

1. Introduction

Organic ligand based synthesis of metal-complexes wherein supramolecular interactions are involved, are at the focal point of research community due to their stunning structural topologies as well as countless applications in wide range of fields [1–4]. The wise choosing of the metal, ligand and careful play of the reaction conditions are of utmost importance in generating these compounds with fascinating supramolecular architectures [5–7]. The artist behind the formation of these supramolecular assemblies from the crystal structures of the compounds is the non-covalent

 doi:10.20944/preprints202408.1099.v1

interactions which are at the heart of the supramolecular chemistry [8–10]. Though these non-covalent interactions are weaker in nature, their collective accumulation have the ability to direct and energetically influence the self-assembly processes of crystal structure and their properties too [11,12]. Therefore, it is desirable to synthesize these kinds of metal-organic compounds and study their self-assemblies involving non-covalent interactions for further understanding and breakthroughs in supramolecular chemistry [13,14]. Different kinds of non-covalent interactions studied in supramolecular chemistry include hydrogen bonding, aromatic π-stacking, metal ion coordination [15–19] etc. Moreover, uncoventional σ-hole and π-hole, C–H···π , anion-π and lone pair (lp)-π interactions have gained interest in recent times [20–25]. Particularly, the anion-π interaction, a non-covalent attractive force between electron-poor aromatic rings and anions, have gained tremendous research interest recently, due to their diverse applications in areas like molecular recognition, catalysis, sensing, and also in designing of new selective anion-receptors [26]. On a similar line, C–H···π interaction (a weak attraction between π system and C-H bond), has also captivated researchers for their ability to guide crystal packing, impact in biology and molecular recognition processes [27–29]. However, hydrogen bonding and aromatic π-stacking is still the most common non-covalent interaction that guides and also energetically influences the formation of supramolecular assembly of metal-organic compounds [30–32]. The tactful utilization of these non-covalent interactions can lead to new crystal systems with desired physical and chemical properties, leading to quite a number of practical applications [33–35]. Multi-component compounds, classified into co-crystals, salts and polymorphs; are crystalline materials composed of two or more components (ions, atoms or molecules) in the same crystal lattice. They have received astounding attention in crystal engineering due to the advancing role of solid state chemistry in pharmaceutical industries, electronic devices and synthetic organic chemistry [36,37]. It is now been proven that both organic and metal-organic multicomponent compounds offer novel solid formulations for active pharmaceutical ingredients, showcasing enhanced features like improved solubility, chemical stability and other mechanical features [38,39].

The utilization of N- and O- donor ligands have gained wide recognitions in supramolecular chemistry of metal-organic compounds owing to the possibility of structural variations along with wide range of applications [40–42]. Notably, pyridine 2,6-dicarboxylic acid [also known as dipicolinic acid, $C_5H_3N(COOH)_2$] (*2,6-PDC*H_2) is a well-established ligand known for its multidentate and bridging ligation [43–47]. It generates stable chelates with metal ions, which can be utilized for the formation of different unconventional non-covalent contacts involving the chelate ring like C–H···π(chelate) interaction [48]. Pyrazole derived ligands like 3,5-dimethyl pyrazole (*Hdmpz*), is a two nitrogen atom containing ligand which generally binds to the metals through the pyridine type N-atom [49–51]. The –NH moiety of the *Hdmpz* ligand allows hydrogen bond formation with the nearby donor and acceptor units that can impact the creation and stability of the overall self-assembly [52]. Metal complexes of pyrazole display a wide range of excellent activities, including anti-cancer [53], catalysis [54,55], and luminescence [56,57] etc. Moreover, coordination complexes involving chelating ligands like ethylene diamine have also gained importance in the development of metal-organic complexes, mostly from the viewpoint of generating intriguing structural topology and applications [58–61].

In recent times, the enclathration of guest molecules in the cavities of the supramolecular hosts has gained a lot of attention because of their potential application in gas storage, catalysis etc. [62–65]. However, the examples, where both host and guest are metal-complexes, were scarce [66,67]. Even rarer is the report of dual enclathration of complex moieties inside the self-assembled host cavities of complexes formed via non-covalent interactions.

In this work, we have described the syntheses and crystal structures of two new coordination complexes of Ni(II) and Zn(II) involving 2,6-PDC moieties and further characterized them using spectroscopic (FT-IR and electronic spectroscopy), elemental and thermogravimetric (TG) analyses. Crystal analysis of compound **1** unveils uncommon dual enclathration of guest complex cationic moieties within the supramolecular host cavity governed by anion–π, π-stacking, N–H···O, C–H···O and O–H···O hydrogen bonding interactions. Presence of various non-covalent interactions involving

 doi:10.20944/preprints202408.1099.v1

aromatic π-systems and chelate ring such as C–H···π(chelate ring), C–H···π(pyridyl) and π-π interactions along with C–H···O and C–H···N hydrogen bonding interactions stabilize the crystal structure of compound **2**. The structure directing role of some non-covalent interactions have been further analyzed theoretically using density functional theory (DFT) calculations, non-covalent interaction (NCI) plot index and quantum theory of atoms in molecules (QTAIM) computational tools. The unconventional C–H···π(chelate ring) interaction have also been established theoretically along with other interactions and their energetic contributions to the stability of the crystal structures of compounds **1** and **2**.

2. Results and Discussion

2.1. Syntheses and General Aspects

$[Ni(2,6\text{-}PDC)_2]_2[Ni(en)_2(H_2O)_2]_2[Ni(en)(H_2O)_4]\cdot 4H_2O$ (**1**) has been prepared by the reaction between one equivalent of $Ni(Ac)_2\cdot 4H_2O$, one equivalent of disodium salt of 2,6-PDC and one equivalent of en at room temperature having de-ionised water as solvent. Similarly, $[Zn(2,6\text{-}PDC)(Hdmpz)_2]$ (**2**) has been synthesized by taking one equivalent of $Zn(Ac)_2\cdot 2H_2O$, one equivalent of disodium salt of 2,6-PDC and two equivalents of Hdmpz at room temperature in de-ionised water medium. Both the compounds **1** and **2** are well soluble in water as well as in common organic solvents. Compound **1** exhibits room temperature magnetic moment of 2.83 BM suggesting the presence of two unpaired electrons in the octahedral Ni(II) centers [68].

2.2. Crystal Structure Analysis

Figure 1 showcases the molecular structure of compound **1,** which crystallizes in triclinic crystal system with $P\bar{1}$ space group. Selected bond lengths and bond angles around the Ni(II) centers have been summarized in Table 1. Compound **1** comprises of five mononuclear hexa-coordinated Ni(II) centers (Ni1-Ni5). Crystal structure analysis of the compound reveals that the site occupancy factors of Ni2 and Ni5 centers are 0.5 each. Ni1 centre is hexa-coordinated with four coordinated water molecules and one bidentate en moiety. The coordination geometry around the cationic Ni1 center is distorted octahedron where the axial sites are occupied by O1 water molecule and N1 atom of en moiety; whereas the equatorial sites are occupied by N2 atom from en moiety and O2, O3 and O4 water molecules.

Cationic Ni2 and Ni5 centers of the compound are crystallographically unique with two water molecules and two bidentate en moieties, respectively. The coordination geometries around the Ni2 and Ni5 centers are ideal octahedron with the water molecules (O5 and O5# for Ni2; O26 and O26# for Ni5) are occupying at the axial sites and N-atoms (N3, N4, N3# and N4# for Ni2; N9, N10, N9# and N10# for Ni5) of en moieties are present at the equatorial sites. Similarly, anionic Ni3 and Ni4 centers are also hexa-coordinated with two tridentate 2,6-PDC moieties. The axial sites of Ni3 centre are occupied by N5 and N6 atoms; whereas, the equatorial sites are occupied by O6, O8, O10 and O11 atoms from the two coordinated 2,6-PDC moieties. Similarly, the axial sites of Ni4 centre are occupied by N7 and N8 atoms; while the equatorial sites are occupied by O14, O16, O18 and O20 atoms from the 2,6-PDC moieties. Moreover, four lattice water molecules (O22, O23, O24 and O25) are also present in the asymmetric unit of the compound. The average Ni–O and Ni–N bond lengths are almost consistent with previously reported similar Ni(II) complexes [69].

 doi:10.20944/preprints202408.1099.v1

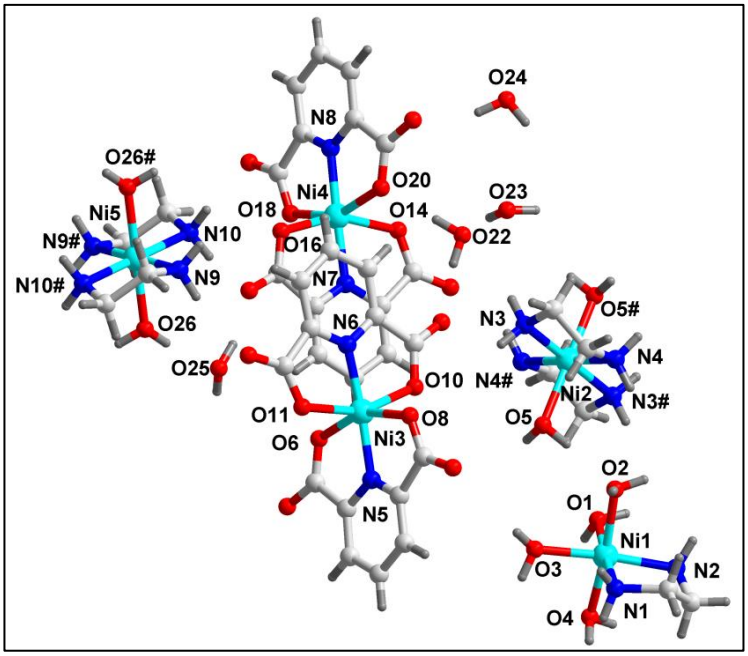

Figure 1. Molecular structure of $[Ni(2,6\text{-}PDC)_2]_2[Ni(en)_2(H_2O)_2]_2[Ni(en)(H_2O)_4]\cdot 4H_2O$ (**1**).

Table 1. Selected bond lengths (Å) and bond angles (°) of Mn(II) and Zn(II) centers in **1** and **2**, respectively.

Compound **1**			
Bond lengths			
Ni1–O3	2.062(2)	Ni3–O11	2.124(2)
Ni1–O4	2.067(2)	Ni3–O6	2.138(2)
Ni1–N2	2.070(3)	Ni3–O8	2.157(2)
Ni1–O1	2.074(2)	Ni4–N7	1.969(2)
Ni1–N1	2.078(3)	Ni4–N8	1.973(2)
Ni1–O2	2.107(2)	Ni4–O16	2.104(2)
Ni2–N3	2.086(3)	Ni4–O18	2.126(2)
Ni2–N4	2.112(3)	Ni4–O14	2.134(2)
Ni2–O5	2.131(2)	Ni4–O20	2.136(2)
Ni3–N6	1.962(2)	Ni5–N9	2.101(3)
Ni3–N5	1.975(3)	Ni5–N10	2.101(3)
Ni3–O10	2.094(2)	Ni5–O26	2.113(2)
Bond angles			
O3–Ni1–O4	87.67(1)	O5–Ni2–O5#	180.0
O3–Ni1–N2	173.90(1)	N6–Ni3–N5	175.13(1)
O4–Ni1–N2	90.18(1)	N6–Ni3–O10	78.48(1)
O3–Ni1–O1	91.37(9)	N5–Ni3–O10	106.39(9)
O4–Ni1–O1	88.66(9)	N6–Ni3–O11	78.09(9)
N2–Ni1–O1	94.28(1)	N5–Ni3–O11	97.04(9)
O3–Ni1–N1	90.07(1)	O10–Ni3–O11	156.55(8)
O4–Ni1–N1	94.33(1)	N6–Ni3–O6	102.00(9)
N2–Ni1–N1	84.40(1)	N5–Ni3–O6	77.91(9)
O1–Ni1–N1	176.73(1)	O10–Ni3–O6	95.36(9)
O3–Ni1–O2	88.18(9)	O11–Ni3–O6	90.50(9)
O4–Ni1–O2	173.01(9)	N7–Ni4–N18	102.51(9)
N2–Ni1–O2	94.49(1)	N8–Ni4–N18	78.16(9)

 doi:10.20944/preprints202408.1099.v1

O1–Ni1–O2	85.81(8)	O16–Ni4–O18	91.11(9)
N1–Ni1–O2	91.30(1)	N7–Ni4–O14	77.54(9)
N3–Ni2–N3#	180.0	N8–Ni4–O14	100.67(1)
N3–Ni2–N4#	96.86(1)	O16–Ni4–O14	156.54(8)
N3–Ni2–N4	83.14(1)	O18–Ni4–O14	95.28(9)
N4–Ni2–N4#	180.0	N7–Ni4–O20	101.64(9)
N3–Ni2–O5	89.34(1)	N8–Ni4–O20	77.66(9)
N3–Ni2–O5#	90.66(1)	O16–Ni4–O20	94.64(9)
N4–Ni2–O5	87.53(9)	O18–Ni4–O20	155.81(8)
N4–Ni2–O5#	92.47(9)	O14–Ni4–O20	88.72(8)
N4#–Ni2–O5	92.48(9)	N9–Ni5–N9#	180.0
N6–Ni3–O8	102.57(9)	N9#–Ni5–N10#	96.32(1)
N5–Ni3–O8	77.50(9)	N9–Ni5–N10	96.32(1)
O10–Ni3–O8	90.72(9)	N10–Ni5–N10#	180.0
O11–Ni3–O8	93.33(9)	N9–Ni5–O26#	91.14(1)
O6–Ni3–O8	155.39(8)	N9#–Ni5–O26#	88.86(1)
N7–Ni4–N8	178.11(1)	N10–Ni5–O26#	84.49(1)
N7–Ni4–O16	79.05(1)	N10–Ni5–O26	95.51(1)
N8–Ni4–O16	102.73(1)	O26–Ni5–O26#	180.0
Compound 2			
Bond lengths			
Zn1–N1	2.013(2)	Zn1–O8	2.154(2)
Zn1–N1#	2.013(2)	Zn1–O8#	2.154(2)
Zn1–N12	2.019(3)		
Bond angles			
N1–Zn1–N1#	105.11(1)	N1–Zn1–O8	91.62(8)
N1–Zn1–N12	127.44(6)	N12–Zn1–O8	76.63(5)
N1#–Zn1–N12	127.44(6)	N1#–Zn1–O8#	91.62(8)
N1–Zn1–O8#	104.65(8)		

Detailed crystallographic analysis unveils that the neighbouring anionic complex moieties of compound **1** are interconnected via anion–π, π–π and C–H···O hydrogen bonding interactions along the crystallographic c axis to form the 1D supramolecular chain (Figure 2). Anion–π interactions are found between the carboxyl O atoms (O13 and O17) and π systems of pyridyl ring of 2,6-PDC having the centroid(C20-C24, N7)···O13 and centroid(C13-C17, N6)···O17 separation distances of 3.36 and 3.49 Å, respectively. The corresponding angles between the respective anions (O13 and O17), centroids and the planes of the aromatic rings are found to be 93.1° and 91.1°, respectively which are nearby to the ideal value of 90°; thereby establishing the strong nature of the anion-π interactions [70]. Aromatic π-stacking interactions are also observed between the aromatic rings of 2,6-PDC moieties having centroid(N8, C27-C31)–centroid(N8′, C27′-C31′) and centroid(N5, C6-C10)–centroid(N5′, C6′-C10′) separations of 3.63 and 3.66 Å, respectively. The corresponding slipped angles; angles between the ring normal and the vector joining the two ring centroids; are found to be 21.5 and 21.9° respectively, thus closely matching the literature value of slipped π-stacking interactions [22]. Moreover, C–H···O hydrogen bonding interactions are observed between the –CH moieties (–C21H21 and –C14H14) and carboxyl O atoms (O6 and O20) of coordinated 2,6-PDC having C14–H14···O20 and C21–H21···O6 distances of 2.73 and 2.51 Å, respectively.

 doi:10.20944/preprints202408.1099.v1

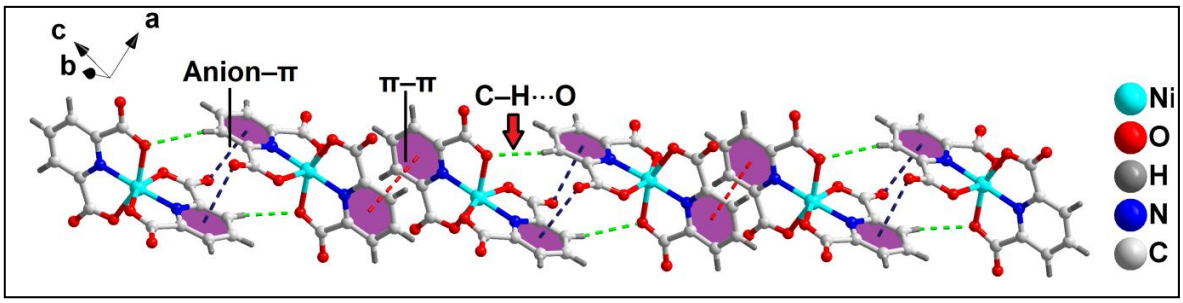

Figure 2. Formation of 1D supramolecular chain of compound **1** assisted by non-covalent anion-π, π-stacking and C–H···O hydrogen bonding interactions along the crystallographic c axis.

Further analysis of **1** discloses unusual dual enclathration of two cationic Ni5 complex moieties within the supramolecular host octameric cavity formed by Ni1, Ni3 and Ni4 complex moieties (Figure 3). The supramolecular host cavity is formed with the help of aforementioned non-covalent anion–π, π-stacking interactions along with N–H···O and O–H···O hydrogen bonding interactions. N–H···O hydrogen bonding interactions are observed between the –NH moiety (–N2H2A′) of coordinated en and carboxyl O atom (O14) of 2,6-PDC having N2–H2A′···O14 distance of 1.97 Å. In addition, O–H···O hydrogen bonding interactions are also observed between the coordinated water molecules and carboxyl O atoms of 2,6-PDC having O2–H2A···O15, O3–H3B···O11 and O4–H4A···O12 distances of 1.87, 1.94 and 1.83 Å, respectively. However, the two enclathrated guest complex cationic moieties are stabilized within the supramolecular host cavity via N–H···O, C–H···O and O–H···O hydrogen bonding interactions. –NH moieties (–N9H9A and–N10H10A) of en from the two guest complex cationic moieties are involved in N–H···O hydrogen bonding interactions with the O12 and O19 atoms of 2,6-PDC having N9–H9A···O12 and N10–H10A···O19 distances of 2.26 and 2.36 Å, respectively. C–H···O hydrogen bonding interaction is also observed between the –C1H1D moiety of en and O26 atom of 2,6-PDC having C1–H1D···O26 distance of 3.00 Å. O–H···O hydrogen bonding interactions are visible between the carboxyl O19 atom of 2,6-PDC and coordinated water molecule (O26) having O26–H26A···O19 distance of 1.93 Å. All the above mentioned non-covalent contacts are analyzed with the help of theoretical methods (vide infra). These enclathrated dual guest complex cationic moieties stabilize the layered assembly of the compound along the crystallographic ac plane (Figure 4).

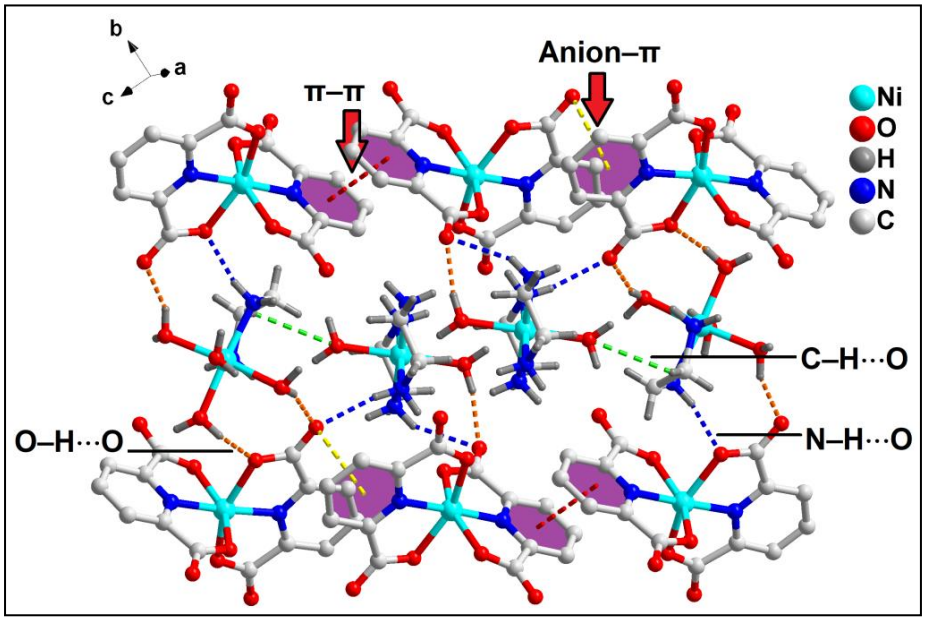

 doi:10.20944/preprints202408.1099.v1

Figure 3. Unusual dual enclathration of guest complex cationic moieties within the supramolecular host cavity of compound **1** stabilized by anion–π, π-stacking, N–H···O, C–H···O and O–H···O hydrogen bonding interactions.

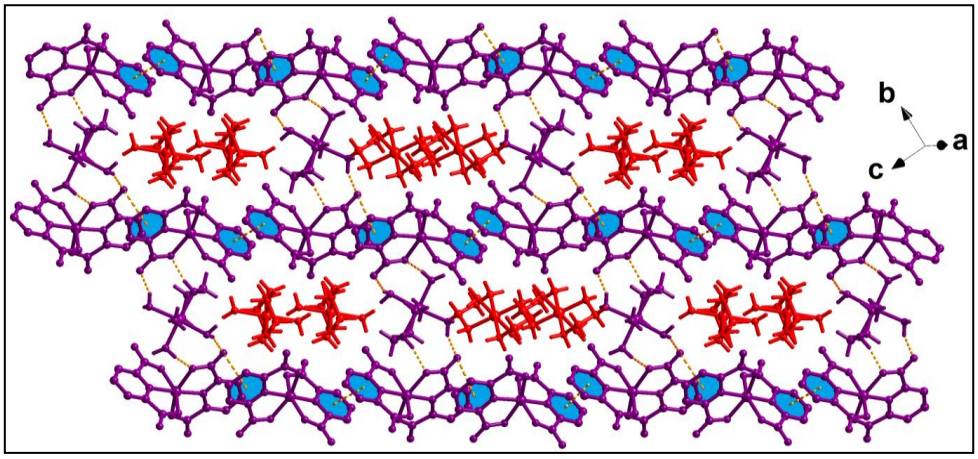

Figure 4. Layered assembly of compound **1** guided by dual enclathration of complex cationic moieties inside the self-assembled host cavity of the compound along the crystallographic ac plane.

Cationic complex moiety (Ni5) of compound **1** is further enclathrated within another supramolecular host cavity assisted by anionic complex moieties (Ni4) and lattice water molecules (O24 and O25) (Figure 5). The supramolecular host cavity is stabilized by O–H···O hydrogen bonding and non-covalent C–H···C interactions. Lattice water molecules (O24 and O25) are involved in O–H···O hydrogen bonding interactions with the carboxyl O atoms (O17 and O21) of coordinated 2,6-PDC of Ni4 complex moieties having O25–H25B···O17, O25–H25A···O24 and O24–H24B···O21 separations of 1.84, 1.92 and 1.89 Å, respectively. In addition, non-covalent C–H···C interactions are observed between the –C28H28 moieties and C27 atoms from 2,6-PDC of two adjacent anionic Ni4 units with C28–H28···C27 distance of 3.48 [C(sp^2)–H28···C(sp^2); C28···C27 = 3.94 Å]. The guest Ni5 complex cationic moieties are interacting with the supramolecular host cavities through N–H···O, O–H···O and C–H···O hydrogen bonding interactions. The –N9H9B moieties from coordinated en of guest complex cationic moieties (Ni5) are involved in N–H···O hydrogen bonding interactions with the carboxyl O18 atoms from 2,6-PDC of two adjacent Ni4 complex units having N9–H9B···O18 separation distance of 2.16 Å; whereas, the –CH (–C34H34B) moieties of en are involved in C–H···O hydrogen bonding interactions with the carboxyl (O17) atom from 2,6-PDC of two neighbouring Ni4 complex units having C34–H34B···O17 distance of 2.72 Å. Moreover, the coordinated water molecules (O26) of the guest moiety are involved in O–H···O hydrogen bonding interactions with the carboxyl (O19) atoms of 2,6-PDC of adjacent host anionic moieties having O19–H19B···O26 distance of 1.93 Å.

Preprints.org (www.preprints.org) | NOT PEER-REVIEWED | Posted: 15 August 2024 doi:10.20944/preprints202408.1099.v1

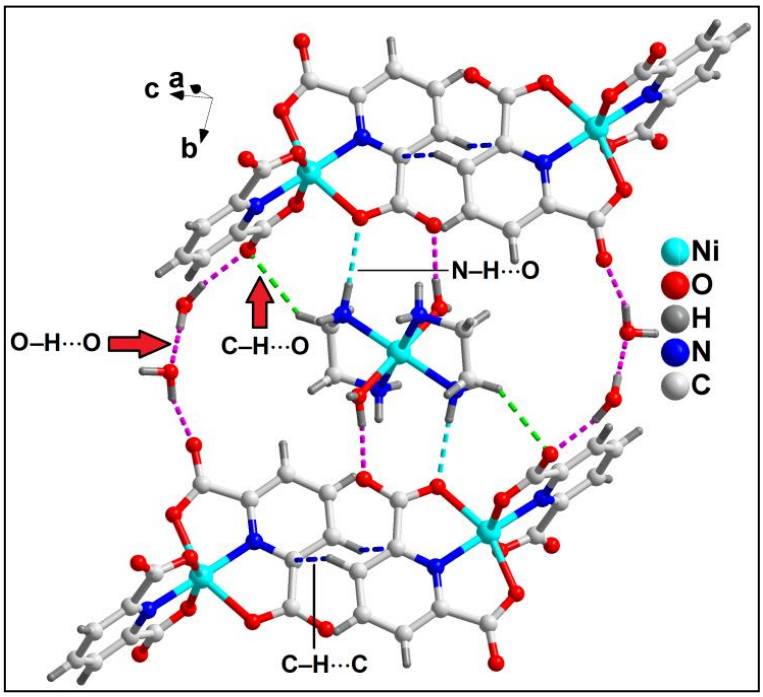

Figure 5. Enclathration of cationic (Ni5) complex moiety within the supramolecular host cavity of compound **1** stabilized by N–H···O, O–H···O and C–H···O hydrogen bonding interactions.

These enclathrated cationic moieties inside the supramolecular host cavities along with C–H···O and O–H···O hydrogen bonding interactions stabilize the layered assembly of the compound along the crystallographic bc plane (Figure 6). C–H···O hydrogen bonding interactions are observed between the –CH moieties and carboxyl O6 atom of 2,6-PDC having C22–H22···O6 separation of 2.93Å. Lattice water molecules (O22, O23 and O24) along with the carboxyl (O7, O13 and O20) O-atoms of 2,6-PDC are involved in O–H···O hydrogen bonding interactions (O22–H22A···O13 = 1.82 Å; O22–H22B···O20 = 1.83 Å; O23–H23A···O22 = 1.89 Å; O23–H23B···O7 = 2.04 Å; O24–H24A···O7 = 1.98 Å), further strengthening the assaembly.

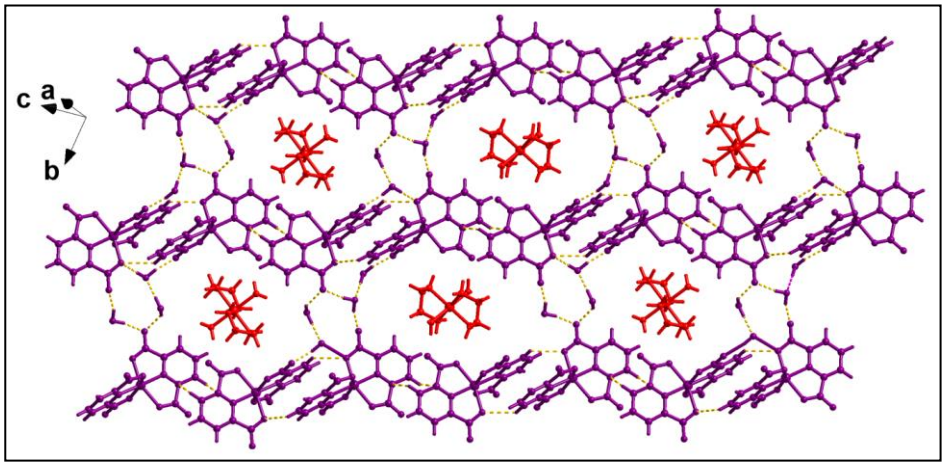

Figure 6. Layered assembly of compound **1** assisted by enclathration of cationic moieties inside self-assembled host cavities along the crystallographic bc plane.

Figure 7 represents the molecular structure of compound **2**. Selected bond lengths and bond angles have been summarized in Table 1. Compound **2** crystallizes in monoclinic crystal system having C2/c space group. In compound **2**, the Zn(II) metal centre is penta-coordinated with two monodentate Hdmpz moieties and one tridentate 2,6-PDC moiety.The coordination geometry around the Zn1 centre in compound **2** is distorted square pyramidal as indicative from the trigonality

 doi:10.20944/preprints202408.1099.v1

index value (τ) of 0.4 [71]. The apical site is taken up by N1 atom from a Hdmpz moiety and the equatorial sites are constituted by coordinated O8, O8# and N12 atoms from the 2,6-PDC moiety & N1# atom from another Hdmpz unit. The equatorial atoms of the Zn1 centre are displaced from the mean equatorial plane with the mean r.m.s. deviation of 0.1120 Å. The average Zn–O and Zn–N bond lengths are almost parallel with the earlier documented Zn(II) complexes [71].

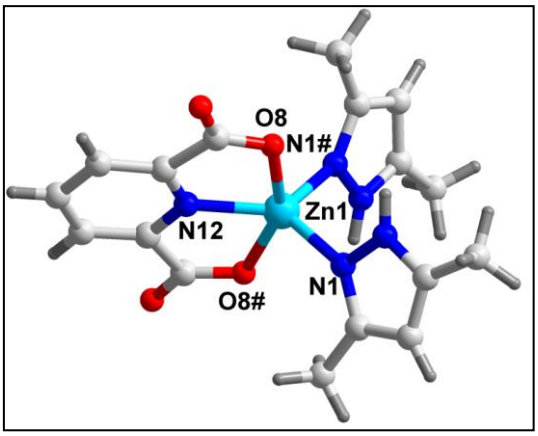

Figure 7. Molecular structure of [Zn(2,6-PDC)(Hdmpz)$_2$] (**2**).

The neighbouring monomeric units of compound **2** are interconnected via non-covalent C–H···O, C–H···N hydrogen bonding interactions in conjunction with π-stacking, C–H···π(chelate ring) [48] and CH···π(pyridyl) interactions to form the 1D supramolecular chain along the crystallographic c axis (Figure 8). C–H···O hydrogen bonding interactions are observed between the –C5H5 moiety of Hdmpz and uncoordinated O10 atom of coordinated 2,6-PDC of adjacent monomeric unit having C–H···O distance of 2.84 Å. In a similar manner, C–H···N hydrogen bonding interactions are observed between the –C4H4A moiety of Hdmpz with the N1 atom of another Hdmpz of adjacent complex unit having C–H···N distance of 2.64 Å. In addition to it, aromatic π-stacking interactions are observed between the aromatic rings of Hdmpz from neighbouring units with Cg-Cg(where Cg is the centroid formed by the atoms C3, C5, C6, N1 and N2) distance of 4.03 Å and slipped angle (angle between the ring normal and the vector joining the ring centroids) 15.9°. C–H···π(pyridyl) interactions have also been observed between the –CH_3 group of Hdmpz and the pyridyl ring of 2,6-PDC coordinated to the metal centre of adjacent monomeric units having C7-Cg_1 and H7B-Cg_1 distances of 3.67 and 2.93 Å, respectively (Cg_1 is the aromatic ring centroid defined by N12, C11, C13, C14, C13′, C11′). The corresponding C–H···π angle is 140.3°, thus revealing the strong nature of the C–H···π interaction [72]. Interestingly, C–H···π(chelate ring) interactions have been equally observed between the –CH_3 moiety of Hdmpz and the chelate ring formed by coordinated 2,6-PDC to the adjacent monomeric Zn(II) metal centres having C4-Cg_2 and H4A-Cg_2 distances of 3.58 and 2.93 Å, respectively (Cg_2 is the aromatic ring centroid defined by (Zn1, O8, C9, C11, N12). A dimer unit of this 1D chain stabilized by aforementioned non-covalent interactions has been taken for theoretical study to prove its existence and energetic significance in the crystal packing (vide infra).

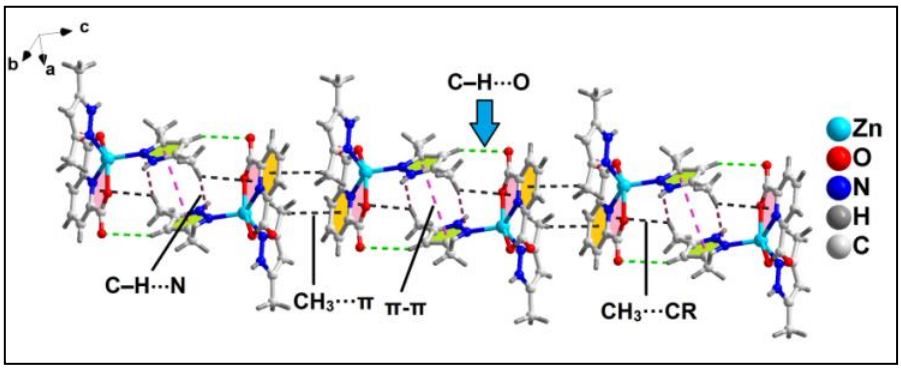

 doi:10.20944/preprints202408.1099.v1

Figure 8. 1D chain of compound **2** involving intermolecular C–H···O, C–H···N hydrogen bonding interactions and π-stacking, CH_3···π(CR) and CH_3···π(pyridyl) interactions along the crystallographic c axis.

Further introspection reveals that the adjacent 1D chains of compound **2** are involved in the formation of a layered assembly along the crystallographic ab plane supported by non-covalent C–H···O and N–H···O hydrogen bonding interactions (Figure 9). The C–H···O interactions are observed between the –CH_3 group of Hdmpz and uncoordinated O10 atom of coordinated 2,6-PDC of neighbouring monomeric unit belonging to the adjacent layer having C7–H7A···O10 distance of 2.63 Å. Similarly, N–H···O interactions, equally responsible for crafting the layered architecture is observed between the –N_2H_2 unit of Hdmpz and uncoordinated O10 atom of 2,6-PDC with N2–H2···O10 distance of 1.96 Å.

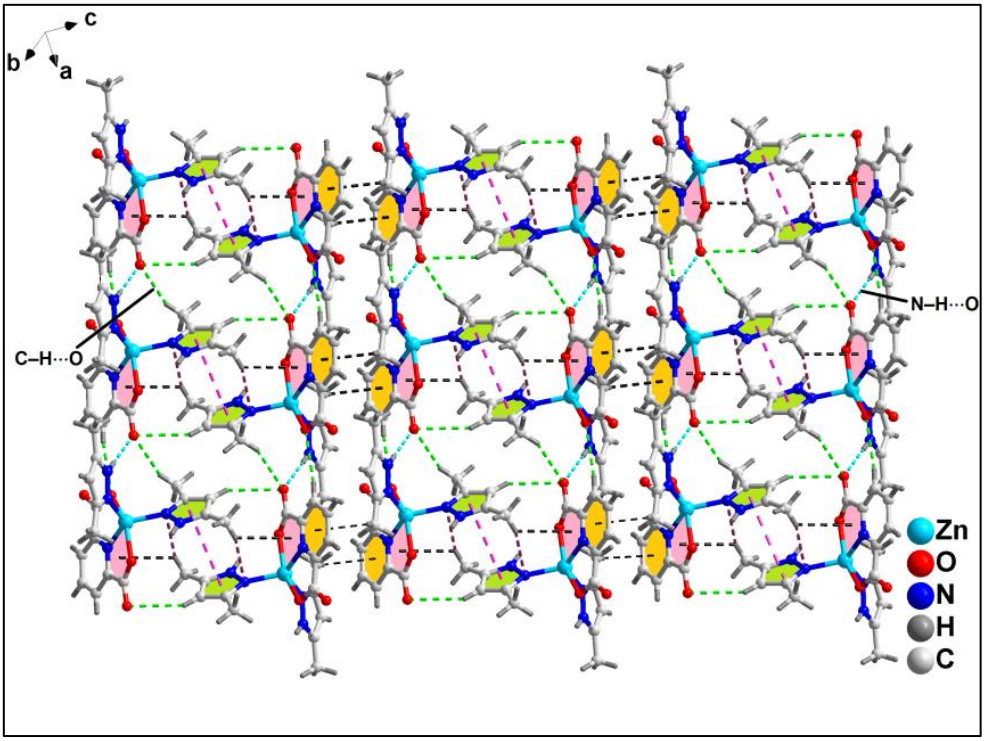

Figure 9. Layered assembly of compound **2** involving C–H···O and N–H···O hydrogen bonding interactions along the crystallographic bc plane.

For compound **2**, formation of a layered assembly along the crystallographic ac plane, aided by non-covalent C–H···π(pyridyl) and C–H···C interactions, is observed (Figure 10). The –CH moiety (–C7H7B) of 2,6-PDC is involved in C–H···π interactions with the π-system of the pyridyl ring of 2,6-PDC having centroid(N12, C11, C11′, C13, C13′,C14)···H7B distance of 2.93 Å. The angle between C7, H7B and the centroid of the pyridyl ring is 132.2° which suggests the strong nature of the interaction [72]. Moreover, non-covalent C–H···C interactions [73–75] are observed between the –CH moieties (–C7H7A and –C7H7B) and C5 atoms of Hdmpz having C7–H7A···C5 and C7–H7B···C5 distances of 3.62 and 3.06 Å respectively [$C(sp^3)$–H7A···$C5(sp^2)$; C7···C5 = 3.633 Å]. In addition, the –C5H5 moiety of Hdmpz is also involved in C–H···C interactions with the C atoms (C5′ and C7) of Hdmpz having C5–H5···C5′ and C5–H5···C7 distances of 3.29 and 3.17 Å respectively [$C(sp^3)$–H7A···$C5(sp^2)$; C7···C5 = 3.633 Å; $C(sp^2)$–H5A···$C(sp^2)$; C5···C5′ = 3.617 Å]. From this assembly, a dimer (responsible for chain propagation) formed by two complex moieties through two C–H···π interactions has been established further by theoretical analysis (vide infra). Selected hydrogen bond distances (Å) and angles (°) for both **1** and **2** have been tabulated in Table 2.

 doi:10.20944/preprints202408.1099.v1

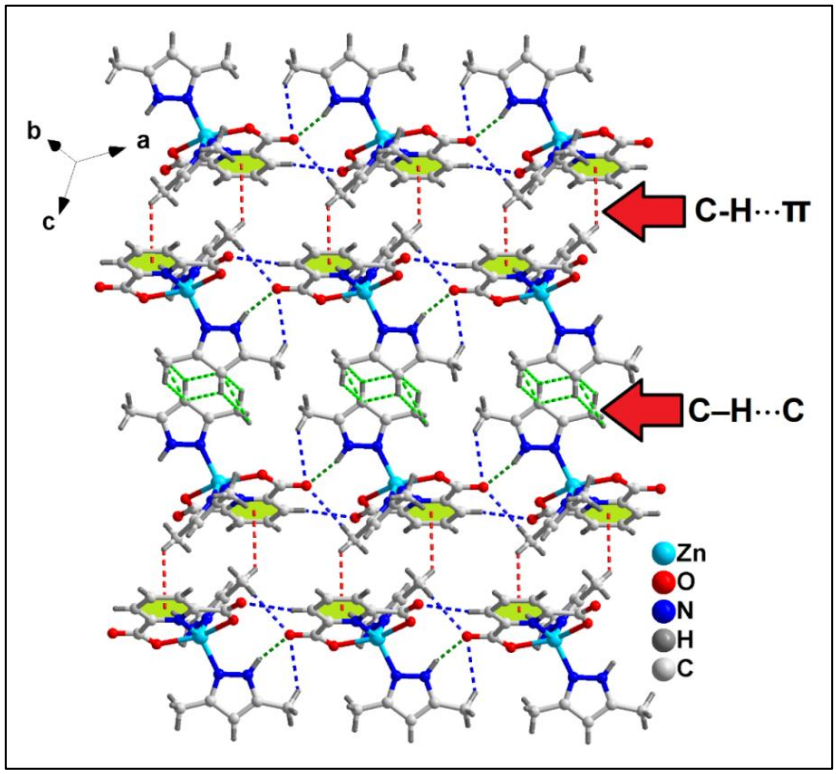

Figure 10. Layered assembly of **2** involving non-covalent C–H···π and C–H···C interactions along the crystallographic ac plane.

Table 2. Selected hydrogen bond distances (Å) and angles (deg.) for compound **1** & **2**.

D–H···A	d(D···A)	d(H···A)	(DHA)		
Compound **1**					
C14–H14···O20	0.95	3.58	2.73	150.8	
C21–H21···O6	0.95	3.27	2.51	136.4	
N2–H2A′···O14	0.91	2.86	1.97	167.4	
O2–H2A···O15	0.88	2.67	1.87	151.5	
O3–H3B···O11	0.87	2.75	1.94	155.2	
O4–H4A···O12	0.88	2.65	1.83	155.3	
N9–H9A···O12	0.91	3.16	2.26	170.1	
N10–H10A···O19	0.91	3.19	2.36	153.3	
C1–H1D···O26	0.99		3.65	3.00	123.4
O26–H26A···O19	0.87	2.77	1.93	163.2	
O25–H25B···O17	0.87	2.69	1.84	167.6	
O25–H25A···O24	0.87	2.78	1.92	177.6	
O24–H24B···O21	0.87	2.74	1.89	162.4	
N9–H9B···O18		0.91	3.05	2.16	169.1
C34–H34B···O17		0.99	3.58	2.72	145.6
O19–H19B···O26	0.87	2.77	1.93	163.3	
C22–H22···O6	0.95	3.36	2.93	108.9	
O23–H23A···O22	0.87	2.76	1.89	170.6	
O23–H23B···O7	0.87	2.74	2.04	136.4	
O24–H24A···O7	0.87	2.83	1.98	167.2	
O22–H22A···O13	0.87	2.68	1.82	171.1	
O22–H22B···O20	0.87	2.70	1.83	177.0	
Compound **2**					

 doi:10.20944/preprints202408.1099.v1

C5–H5···O10	0.95	3.63	2.84	142.2
C4–H4A···N1	0.98	3.54	2.64	153.0
C7–H7A···O10	0.97	3.51	2.63	149.9
N2–H2···O10	0.88	2.79	1.96	156.6

2.3. Spectral Studies

2.3.1. FT-IR Spectroscopy

The FT-IR spectra of compounds **1** and **2** have been determined in the region 4000-500 cm^{-1} (Figure S1). The broad absorption band in the spectrum of compound **1** in the region 3200-3600 cm^{1} can be attributed to the O–H stretching vibrations of the coordinated and lattice water molecules [76,77]. FT-IR spectrum of compound **1** also exhibit absorption bands owing to ρ_r (H_2O) (710 cm^{-1}) and ρ_w (H_2O) (670 cm^{-1}) supporting the presence of coordinated water molecules [78]. The bands at around 1616 and 1593 cm^{-1} in the FTIR spectra of **1** and **2**, respectively, can be designated as the asymmetric stretching vibrations of the carboxylate groups of 2,6-PDC moieties; while the bands for symmetric stretching vibrations of 2,6-PDC of both the compounds occur at 1381 and 1351 cm^{-1}. The difference between asymmetric and symmetric stretching vibrations of the carboxylate groups of 2,6-PDC were found to be 235 and 242 cm^{-1} for compounds **1** and **2**, respectively, implying the monodentate coordination of the carboxylate groups to the respective metal centers [79]. The absorption peaks at 1593, 1108 and 774 cm^{-1} in the FTIR spectrum of **1** are due to the –NH stretching, C–N stretching and $–CH_2$ rocking vibrations of coordinated en moieties, respectively [80,81]. The band at around 3235 cm^{-1} in the spectrum of **2** can be assigned to the N–H stretching vibrations of coordinated Hdmpz moiety [82,83] present in the compound. The C–H stretching vibrations of the coordinated Hdmpz are observed in the region of 2970–2770 cm^{-1} [84]. The peaks at 1425, 1273 and 1163 cm^{-1} in **2** are due to the C–N, N–N and C=N stretching vibrations of Hdmpz rings respectively [85].

2.3.2. Electronic Spectroscopy

Both solid and aqueous phase electronic spectra of the compounds have been determined. (Figures S2 and S3). The spectra of the compounds supports the presence of distorted octahedral Ni(II) and distorted square pyramidal Zn(II) centers in the compounds **1** and **2**, respectively [86–91]. The absorption peaks for the $\pi \rightarrow \pi^*$ transition of the aromatic ligands are found at the desired positions [92,93]. The simlarity in the absorption bands in both the phases of the spectra of compounds **1** and **2** reflects lesser deformation in structural aspects of the compounds in both the phases [94,95].

2.4. Thermogravimetric Analysis

The thermogravimetric data of the compounds **1** and **2** were determined in the temperature range 25–800 °C in N_2 atmosphere keeping the heating rate at 10°C/min (Figure S4). For compound **1**, firstly the lattice and coordinated water molecules get decomposed within the temperature range 35–148°C with the observed weight loss of 13.44% (calc. = 14.30%) [96,97]. In the final step, the coordinated en moieties and all the PDC moieties are lost within the temperature range 170–345°C (obs. =68.09%; calc. =66.94%) [98,99]. In case of compound **2**, the first step of decomposition is found at 70-405°C, corroborating to a mass loss of 44.51% (calcd. = 45.48%) for two coordinated Hdmpz moiety [100,101]. Finally, at 410-580°C mass loss of 40.95% (calcd. = 39.26%) is incurred, corresponding to the loss of PDC moiety [102,103].

2.5. Theoretical Study

The theoretical DFT study is focused on the study of several supramolecular assemblies observed in the solid state of compounds **1** and **2** that are relevant to understand their crystal packing. Compound **1** can be regarded as a salt composed by dicationic and dianionic Ni(II) complexes.

 doi:10.20944/preprints202408.1099.v1

Therefore, non-directional electrostatic forces are dominant. However, the orientation of the molecules is finely tuned by other weaker interactions like π-stacking or H-bonds. As a representative assembly, we have computed the tetramer shown in Figure 11, composed by two cations and two anions. The formation energy is quite large (–72.4 kcal/mol) due to the Coulombic attraction between the ion-pairs. The combined QTAIM/NCI plot analysis of the tetramer is represented in Figure 11 and shows that the π-stacking interaction is characterized by three bond critical points (CPs, represented as small red spheres) and bond paths (orange lines) interconnecting three C-atoms of the aromatic ligands. The anion···π interactions described above in Figures 2 and 3 are not revealed by the QTAIM analysis (absence of CPs connecting the O-atom to the ring). However, the NCI plot method, that is very useful to reveal interactions in real space, shows a large RDG (reduced density gradient) isosurface that extends to the region between the carboxylate group and the aromatic ring, thus supporting the existence of anion(O)···π interaction. The combined QTAIM/NCI Plot analysis also reveals the existence of a network of H-bonding contacts. In particular, there are six N–H···O, two O–H···O and four C–H···O hydrogen bonds with a total contribution of –31.9 kcal/mol, which was evaluated using the QTAIM by means of the potential energy density (V_r) at the bond CPs that characterize the H-bonds (see section 3.3). It should be mentioned that this energy is free from the influence of ion-pair effects. The strongest H-bond corresponds to the O–H···O due to the enhanced acidity of the Ni-coordinated water protons and the anionic nature of the acceptor.

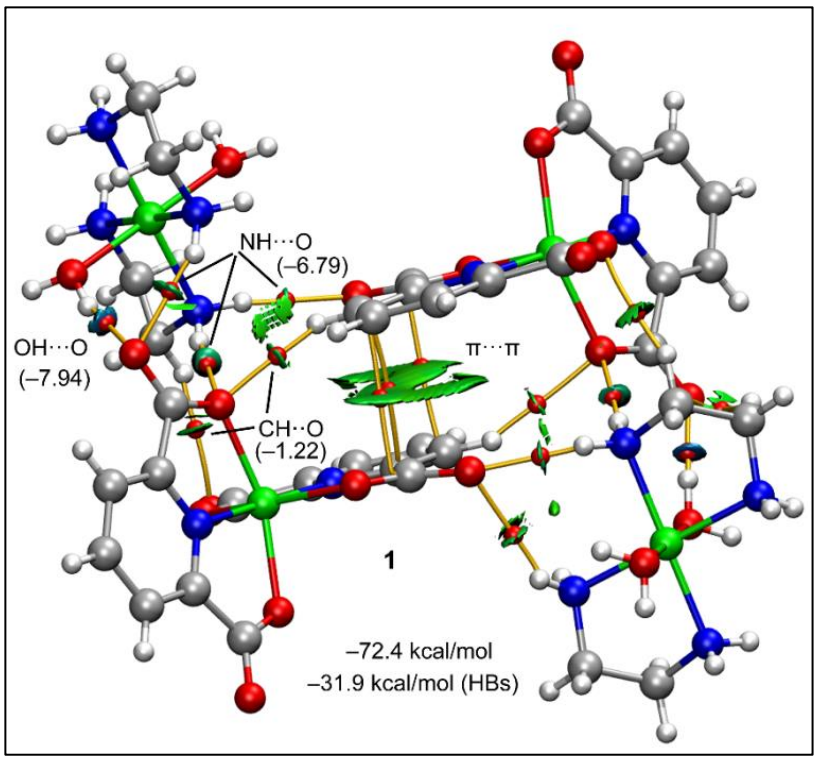

Figure 11. QTAIM (bond CPs in red and bond paths as orange lines) and NCIplot analyses (RDG = 0.6, $\varrho_{cut\text{-}off}$ = 0.04, color range –0.04 a.u. ≤ (signλ_2)ϱ ≤ 0.04 a.u. for the π-stacking (a) and H-bonded (b) assemblies of compound **1**. The H-bonding energies evaluated using the Vr energy predictor are indicated in parenthesis.

In compound **2**, we have studied the π-stacking, C–H···π and hydrogen bonding interactions observed in its solid state architecture. First, we have computed the MEP surface (Figure 12) of compound **2**, showing that the maximum is located at the -NH group of the coordinated pyrazole ligand (+48 kcal/mol). The MEP is also large and positive at the H-atoms of the methyl groups (+23 kcal/mol). The MEP minimum is located at the non-coordinated O-atom of the carboxylic group (–54 kcal/mol) of 2,6-PDC ligand. The MEP is positive over the centre of the pyrazole ring (+10 kcal/mol) and small and negative over the aromatic ring of 2,6-PDC ligand (–5 kcal/mol). The positive MEP

 doi:10.20944/preprints202408.1099.v1

value at the methyl H-atoms and negative MEP value over the aromatic ring of 2,6-PDC ligand showcases the feasibility of interactions like C–H···π.

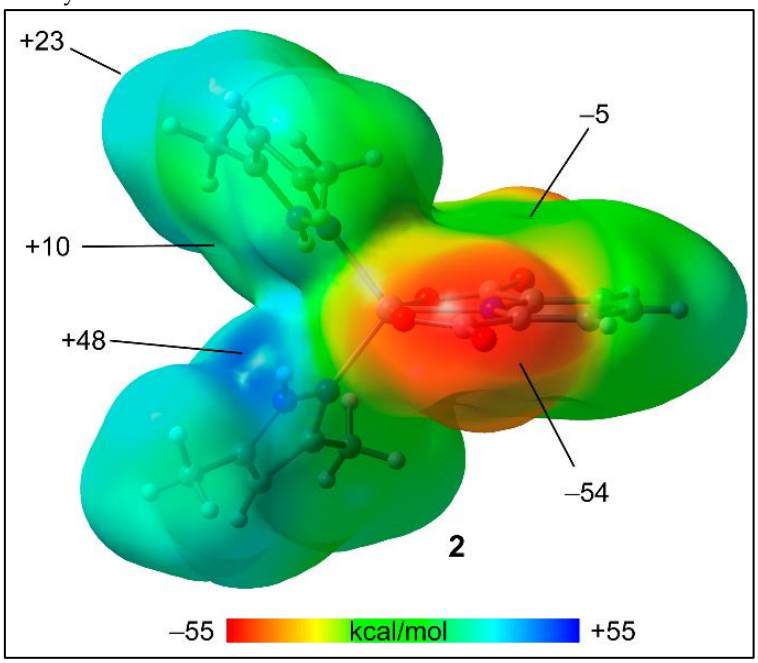

Figure 12. MEP surface of compound **2**. The values at selected points of the surface are given in kcal/mol. Isovalue 0.001 a.u.

Figure 13 shows two interesting assemblies (centrosymmetric dimers) retrieved from the solid state of compound **2**. The first assembly (Figure 13a) is used to emphasize the existence of π-stacking between the pyrazole rings that is characterized by two bond CPs connecting the one carbon atom of one ring to the N-atom of the adjacent ring and vice versa. It is further characterized by an extended green RDG isosurface, as typical in π-stacking interactions. More remarkably, the combined QTAIM/NCI plot analysis shows the existence of a large RDG isosurface located between one methyl group of Hdmpz moiety and the five membered chelate ring(CR) involving the Zn centre and coordinated 2,6-PDC moiety. This is further characterized by a bond CP and bond path connecting one H-atom of the methyl group to the O-atom of the chelate ring. Although the QTAIM only shows one CP connecting the methyl and one atom of the CR, the shape and size of the RDG isosurface clearly supports the participation of all atoms of the CR, evidencing for the C–H···π(chelate ring) interaction. Finally, the QTAIM/NCI plot also shows two additional contacts (C–H···O and C–H···N) each one characterized by a bond CP and bond path connecting two CH groups (aliphatic and aromatic) to the N or O-atoms of the Hdmpz and 2,6-PDC ligands, respectively). The contributions of these H-bonds have been estimated using the V_r energy predictor, which are –1.19 kcal/mol and –0.54 kcal/mol for the C–H···N and C–H···O contacts, respectively. The total interaction energy of this self-assembled dimer is large and negative (–19.7 kcal/mol) due to this intricate combination of interactions. Figure 13b shows the other self-assembled dimer that is governed by two C–H···π(pyridyl) or CH_3···π interactions. This type of dimer is important for the formation of the 2D layered assembly in compound **2** (Figure 10 above). The QTAIM/NCI plot analysis shows that the CH_3···π interaction is characterized by a bond CP and bond path connecting one H-atom of the methyl group to one C-atom of the pyridine ring. Again, the NCI plot analysis describes better the π-nature of the interaction, showing an extended green RDG isosurface that embraces most of the π-cloud of the pyridine ring. The interaction energy is –8.8 kcal/mol, thus revealing that each CH_3···π interaction is –4.4 kcal/mol, in line with the positive MEP at the methyl groups of pyrazole and the negative MEP value over the 2,6-PDC ligand (see Figure 12).

Preprints.org (www.preprints.org) | NOT PEER-REVIEWED | Posted: 15 August 2024 doi:10.20944/preprints202408.1099.v1

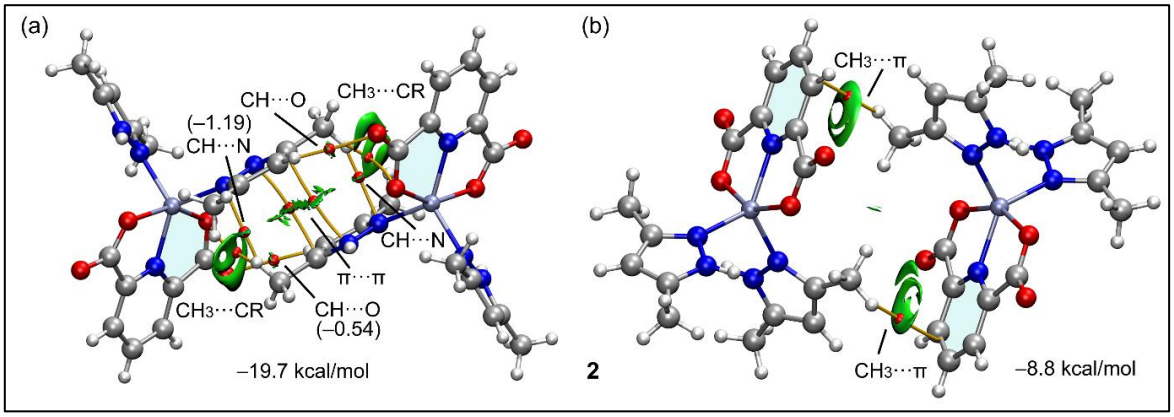

Figure 13. QTAIM (bond CPs in red and bond paths as orange lines) and NCIplot analyses (RDG = 0.6, $\varrho_{cut\text{-}off}$ = 0.04, color range –0.04 a.u. ≤ (signλ_2)ϱ ≤ 0.04 a.u. for the π-stacking (a) and $CH_3\cdots\pi$ (b) assemblies of compound **2**. The H-bonding energies evaluated using the Vr energy predictor are indicated in parenthesis.

3. Materials and Methods

All the chemicals viz. $Ni(Ac)_2{\cdot}4H_2O$, $Zn(Ac)_2{\cdot}2H_2O$, ethylene diamine (en), 2,6-pyridinedicarboxylic acid (2,6-$PDCH_2$) and 3,5-dimethylpyrazole (Hdmpz) utilized in this work were procured from Sigma Aldrich and Merck (India) Ltd. and used as it is. Elemental analyses were performed with the help of Perkin Elmer 2400 Series II CHN analyzer. Bruker Alpha (II) Infrared spectrophotometer (frequency range 4000-500 cm^{-1}) was used to record the FT-IR spectra of the compounds. Shimadzu UV-2600 spectrophotometer was utilized for the purpose of recording the diffuse-reflectance electronic spectra of the compounds. $BaSO_4$ powder was used as reference (100% reflectance) for solid phase UV-Vis-NIR spectra. Room temperature magnetic susceptibilities were determined at 300 K in Sherwood Mark 1 Magnetic Susceptibility balance following Evans method. Thermogravimetric studies were conducted under N_2 gas flow, utilizing Mettler Toledo TGA/DSC1 STAR^e system (heating rate = 10°C min^{-1}).

3.1. Syntheses

3.1.1. Synthesis of $[Ni(2,6\text{-}PDC)_2]_2[Ni(en)_2(H_2O)_2]_2[Ni(en)(H_2O)_4]{\cdot}4H_2O$ (1)

$Ni(Ac)_2{\cdot}4H_2O$ (0.248g, 1 mmol) and disodium salt of 2,6-PDC (0.211 g, 1mmol) were dissolved in 10 mL of distilled water in a round bottomed flask and the solution was mechanically stirred at room temperature for one hour. To the resulting green colored solution, en (0.06 mL, 1mmol) was added slowly and stirring continued for another two hours (Figure 14). The final solution was then kept unperturbed at lower temperature (2-4°C) for crystallization. Green colored block shaped single crystals, suitable for single crystal X-ray diffraction studies, were obtained after several days. Yield: 1.105 g (88%). Anal. calcd. For $C_{34}H_{56}N_{10}Ni_4O_{26}$: C, 32.52%; H, 4.50%; N, 11.16%; Found: C, 32.41%; H, 4.42%; N, 11.04%. IR (KBr pellet, cm^{-1}): 3410 (br), 3304 (w), 2961 (sh), 2895 (sh), 2377 (w), 2002 (w), 1933 (w), 1616 (s), 1593 (m), 1426 (m), 1381 (s), 1278 (s), 1108 (m), 1073 (m), 1029 (s), 915 (m), 821 (w), 774 (s), 730 (m), 670 (m), 595 (w), 542 (w) (s, strong; m, medium; w, weak; br, broad; sh, shoulder).

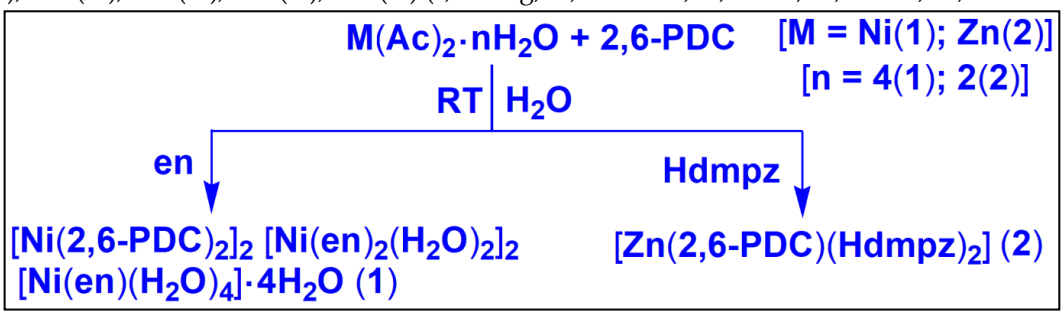

 doi:10.20944/preprints202408.1099.v1

Figure 14. Syntheses of the compounds **1** and **2**.

3.1.2. Synthesis of [Zn(2,6-PDC)(Hdmpz)$_2$] (2)

A mixture of Zn(Ac)$_2$·2H$_2$O (0.219g, 1mmol) and disodium salt of 2,6-PDC (0.211 g, 1mmol) were dissolved in 10 mL of de-ionised water and allowed to stir mechanically in a round bottomed flask at room temperature for one hour. To the resulting colorless solution, Hdmpz (0.192 g, 2 mmol) was added slowly and stirring continued for another two hours (Figure 14). The resulting solution was then kept undisturbed for crystallization in a refrigerator below 4°C. Block shaped colorless single crystals, suitable for single crystal X-ray diffraction studies, were obtained after several days. Yield: 0.368 g (87%). Anal. calcd. For $C_{17}H_{19}N_5O_4Zn$: C, 48.30%; H, 4.53%; N, 16.57%; Found: C, 48.19%; H, 4.41%; N, 16.49%. IR (KBr pellet, cm^{-1}): 3440 (br), 3235 (sh), 3052 (w), 2969(w), 2821 (w), 2750 (w), 1646 (s), 1593 (s), 1425 (m), 1351 (s), 1273 (m), 1163 (m), 1057 (m), 1027 (w), 898 (m), 867 (w), 806 (m), 722 (s), 570 (w) (s, strong; m, medium; w, weak; br, broad; sh, shoulder).

3.2. Crystallographic Data Collection and Refinement

Crystal structures of the compounds **1** and **2** were ascertained on D8 Venture diffractometer, with a Photon III 14 detector, utilizing an Incoatec high brilliance IμS DIAMOND Cu tube equipped having an Incoatec Helios MX multilayer optics. Data reduction and cell refinements were carried out using the Bruker APEX3 program [104]. SADABS is used to perform semi-empirical absorption correction, as well as scaling and merging the different datasets for the wavelength [104]. Crystal structures were solved by direct method and refined by full matrix least squares technique with SHELXL-2018/3 [105] using the WinGX [106] platform available for personal computers. All non-hydrogen atoms were refined with anisotropic thermal parameters by full-matrix least squares calculations on F2. Hydrogen atoms were inserted at calculated positions and refined as riders. The structural diagrams were drawn with Diamond 3.2 [107]. Crystallographic results for the compounds are summarized in Table 3. The crystallographic data of compounds **1** and **2** are provided in Table 3, with CCDC deposition numbers cited in Appendix A.

Table 3. Crystallographic data and structure refinement details for **1** and **2**.

Parameters	**1**	**2**
Formula	$C_{34}H_{56}N_{10}Ni_4O_{26}$	$C_{17}H_{19}N_5O_4Zn$
Formula weight	1255.72	422.74
Temp, [K]	100(2)	100(2)
Crystal system	Triclinic	Monoclinic
Space group	$P\bar{1}$	C2/c
a, [Å]	8.9375(7)	13.9543(16)
b, [Å]	12.8596(10)	9.4508(11)
c, [Å]	21.1687(17)	13.968(2)
α, [°]	85.416(3	90
β, [°]	82.686(2)	111.638(2)
γ, [°]	89.928(3)	90
V [Å^3]	2405.4(3)	1712.3(4)
Z	2	4
Absorption coefficient (mm^{-1})	2.641	.315
F(0 0 0)	1300	872
D (calcd), [Mg/m^3]	1.734	1.640
Index ranges	−10≤h≤10, −15≤k≤15, −0≤l≤25	−16≤h≤16, −11≤k≤11,−16≤l≤16
Crystal size, [mm^3]	0.31 × 0.28 × 0.15	0.21 × 0.16 × 0.13
θ range, [°]	6.10 to 68.28	3.40 to 68.17
Independent Reflections	8443	1491
Reflections collected	8519	1489

 doi:10.20944/preprints202408.1099.v1

Refinement method	Full-matrix	Full-matrix
least-squares on F^2	least-squares on F^2	
Data/restraints/ parameters	8519/0/692	1491/0/126
Goodness-of-fit on F^2	1.085	1.175
Final R indices [I >2σ(I)]	R1 = 0.0559, wR2 = 0.1573	R1 = 0.0419, wR2 = 0.1139
R indices (all data)	R1 = 0.0563, wR2 = 0.1577	R1 = 0.0419, wR2 = 0.1139
Largest hole and peak [e·Å^{-3}]	1.27 and -0.77	0.48 and -0.71

3.3. Computational Methods

The single point calculations were carried out using the Turbomole 7.7 program [108] and the PBE0[109]-D3[110]/def2-TZVP[111] level of theory. The crystallographic coordinates have been used to evaluate the interactions in compounds **1** and **2** since we are interested to study the H-bond contacts as they stand in the solid state. The Bader's "Atoms in molecules" theory (QTAIM) [112] and noncovalent interaction plot (NCI Plot) [113] were used to study the interactions discussed herein using the Multiwfn program [114] and represented using the VMD visualization software [115]. For the calculation of the H-bond energies, we used the equation proposed by Espinosa et al (E = ½Vr) [116]. For the calculation of the binding energy we used the supramolecular approach, where the sum of energies of the monomers was subtracted to the energy of the assembly. For the representation of the MEP surface, the 0.001 a.u. isosurface was used to emulate the van der Waals surface.

4. Conclusions

Two new Ni(II) and Zn(II) coordination compounds viz.[Ni(2,6-PDC)$_2$]$_2$[Ni(en)$_2$(H$_2$O)$_2$]$_2$[Ni(en)(H$_2$O)$_4$]·4H$_2$O (**1**) and [Zn(2,6-PDC)(Hdmpz)$_2$] (**2**) (where, 2,6-PDC = 2,6-pyridinedicarboxylate, en = ethylene-1,2-diamine, Hdmpz = 3,5-dimethyl pyrazole) have been synthesized and characterized using single crystal X-ray diffraction technique as well as spectroscopic (FT-IR, electronic), elemental and thermogravimetric analyses. Compound **1** crystallizes as a multicomponent Ni(II) compound with five discrete complex moieties; whereas, compound **2** is a mononuclear compound of Zn(II). Crystal structure analysis of compound **1** reveals the unusual dual enclathration and also single enclathration of complex cationic moieties within the supramolecular host cavities. Presence of unconventional C–H···π(chelate ring) interactions and C–H···O, C–H···N hydrogen bonding, π-stacking, C–H···π(pyridyl) interactions stabilize the crystal structure of compound **2**. These non-covalent interactions have been further studied theoretically using density functional theory (DFT) calculations, and a combination of QTAIM and NCI plot methods. The computational study showcases that π-stacking or H-bonds finely tunes the directionality of compound **1** amidst the strong non-directional electrostatic forces. They also reveal the existence of energetically significant π-stacking, C–H···π(chelate ring) and C–H···π(pyridyl) interactions in compound **2**.

Supplementary Materials: The following supporting information can be downloaded at the website of this paper posted on Preprints.org, Figure S1: FT-IR spectra of compounds **1** and **2**; Figure S2: (a) UV-Vis-NIR spectrum of **1**, (b) UV-Vis spectrum of **1**; Figure S3: (a) UV-Vis-NIR spectrum of **2**, (b) UV-Vis spectrum of **2**; Figure S4: Thermogravimetric curves of the compounds **1** and **2**.

Author Contributions: Conceptualization, A.F. and M.K.B.; methodology, A.F. and M.K.B.; software, A.F. and R.M.G.; formal analysis, A.F.; investigation, K.K.D.; P.S.; S.B. and R.M.G.; data curation, M.B.-O.; writing—original draft preparation, K.K.D.; writing—review and editing, M.K.B.; visualization, A.F.; supervision, M.K.B.; project administration, A.F. and M.K.B.; funding acquisition, A.F. and M.K.B. All authors have read and agreed to the published version of the manuscript.

Funding: Financial supports obtained from SERB-SURE (Grant number: SUR/2022/001262); In-House Research Project (IHRP), Cotton University [Grant number: CU/Dean/R&D/2019/02/23] and the Gobierno de Espana, MICIU/AEI (projects No. EQC2018-004265-P and PID2020-115637GB-I00) are gratefully acknowledged. K.K.D acknowledges CSIR [09/1236(16497)/2023-EMR-I], Govt. of India for Junior Research Fellowship (JRF). SB thanks CSIR [09/1236(17224)/2023-EMR-I], Govt. of India for Junior Research Fellowship (JRF). The authors thank IIT, Guwahati for TG data.

 doi:10.20944/preprints202408.1099.v1

Data Availability Statement: Data are contained within the article and supplementary materials.

Conflicts of Interest: The authors declare no conflict of interest. The funders had no role in the design of the study; in the collection, analyses, or interpretation of data; in the writing of the manuscript; or in the decision to publish the results.

Appendix A

CCDC 2213593 and 2213594 contains the supplementary crystallographic data for the compounds **1** and **2**. These data can be obtained free of charge at http://www.ccdc.cam.ac.uk or from the Cambridge Crystallographic Data Centre, 12 Union Road, Cambridge CB2 1EZ, UK; fax: (+44) 1223-336-033; or E-mail: deposit@ccdc.cam.ac.uk.

References

1. Lv, Q.; Yu, R.; Shi, R.; Tan, Z.A. Recent Progress in Organic–Metal Complexes for Organic Photovoltaic Applications. *Mater. Chem. Front.* **2023**, *7*, 5063–5103.
2. Ding, H.; Deng, X.; Liu, X.; Shang, W.; Du, X.; Wang, S.; Liu, X.; Chen, X.; Liu, H.; Su, H. Exploring Multi-Stimuli-Responsive Pt(II) Complexes: Supramolecular Self-Assembly, Lysosome-Specific Targeted Photodynamic Therapy and Photodegradation of Organic Pollutants. *Inorg. Chem. Front.* **2024**, *11*, 1693–1702.
3. Dey, N.; Haynes, C.J. Supramolecular Coordination Complexes as Optical Biosensors. *ChemPlusChem* **2021**, *86*, 418–433.
4. Malenov, D.P.; Zarić, S.D. Stacking Interactions of Aromatic Ligands in Transition Metal Complexes. *Coord. Chem. Rev.* **2020**, *419*, 213338.
5. Ma, J.F.; Liu, J.F.; Xing, Y.; Jia, H.Q.; Lin, Y.H. Networks with Hexagonal Circuits in Coordination Polymers of Metal Ions (Zn^{II}, Cd^{II}) with 1,1′-(1,4-Butanediyl)bis(Imidazole). *J. Chem. Soc., Dalton Trans.* **2000**, 2403–2407.
6. Aakeröy, C.B.; Champness, N.R.; Janiak, C. Recent Advances in Crystal Engineering. *CrystEngComm* **2010**, *12*, 22–43.
7. Mirzaei, M.; Eshtiagh-Hosseini, H.; Bolouri, Z.; Rahmati, Z.; Esmaeilzadeh, A.; Hassanpoor, A.; Bauza, A.; Ballester, P.; Barceló-Oliver, M.; Mague, J.T.; Notash, B. Rationalization of Noncovalent Interactions within Six New M^{II}/8-Aminoquinoline Supramolecular Complexes (M^{II} = Mn, Cu, and Cd): A Combined Experimental and Theoretical DFT Study. *Cryst. Growth Des.* **2015**, *15*, 1351–1361.
8. Kumar, P.; Banerjee, S.; Radha, A.; Firdoos, T.; Sahoo, S.C.; Pandey, S.K. Role of Non-Covalent Interactions in the Supramolecular Architectures of Mercury (II) Diphenyldithiophosphates: An Experimental and Theoretical Investigation. *New J. Chem.* **2021**, *45*, 2249–2263.
9. Singh, Y.; Patel, R.N.; Patel, S.K.; Jadeja, R.N.; Patel, A.K.; Patel, N.; Roy, H.; Kumar, P.; Butcher, R.J.; Jasinski, J.P.; Cortijo, M. Non-Covalent Interactions Governing the Supramolecular Assembly of Copper (II) Complexes with Hydrazone-Type Ligand: Experimental and Quantum Chemical Study. *Polyhedron* **2021**, *200*, 115142.
10. Talreja, S.; Tiwari, S. Supramolecular Chemistry: Unveiling the Fascinating World of Non-Covalent Interactions and Complex Assemblies. *J. Pharm. Pharmacol. Res* **2023**, *7*, 133–139.
11. Chauhan, C.; Kumar, S.; Kumar, R.; Saini, A.; Aree, T. Synergistic Effects of Steric Constraints and Non-Covalent Interactions in Copper(II) Chloro-Nitro-Benzoato Complexes: Synthesis, Structural Characterization, Theoretical Investigations, Antimicrobial Studies, and Molecular Docking Analyses. *New J. Chem.* **2024**, *48*, 3829–3848.
12. Singh, J.; Kim, H.; Chi, K.W. Non-Covalent Interaction-Directed Coordination-Driven Self-Assembly of Non-Trivial Supramolecular Topologies. *Chem. Rec.* **2021**, *21*, 574–593.
13. Sadhukhan, A.; Brandão, P.; Saha, S.; Mal, D.; Sepay, N. Insight into Non-Covalent Interactions in 1D Gd-Based Coordination Polymer for Solid-State Self-Assembly through a New Supramolecular Synthon. *J. Mol. Struct.* **2023**, *1272*, 134204.
14. Borovik, A.S. The Use of Non-Covalent Interactions in the Assembly of Metal/Organic Supramolecular Arrays. *Comments Inorg. Chem.* **2002**, *23*, 45–78.

15. Gou, L.; Wu, Q.R.; Hu, H.M.; Qin, T.; Xue, G.L.; Yang, M.L.; Tang, Z.X. An Investigation of the Positional Isomeric Effect of Terpyridine Derivatives: Self-Assembly of Novel Cadmium Coordination Architectures Driven by N-Donor Covalence and π···π Non-Covalent Interactions. *Polyhedron* **2008**, *27*, 1517–1526.
16. Steiner, T. The Hydrogen Bond in the Solid State. *Angew. Chem., Int. Ed.* **2002**, *41*, 48–76.
17. Buckingham, A.D.; Del Bene, J.E.; McDowell, S.A.C. The Hydrogen Bond. *Chem. Phys. Lett.* **2008**, *463*, 1–10.
18. Janiak, C. A Critical Account on π–π Stacking in Metal Complexes with Aromatic Nitrogen-Containing Ligands. *J. Chem. Soc., Dalton Trans.* **2000**, 3885–3896.
19. Lehn, J.M.; Atwood, J.L.; Davies, J.E.D.; MacNicol, D.D.; Vogtle, F. *Comprehensive Supramolecular Chemistry*; Pergamon: Oxford, UK, 1996.
20. Politzer, P.; Murray, J.S.; Clark, T.; Resnati, G. The σ-Hole Revisited. *Phys. Chem. Chem. Phys.* **2017**, *19*, 32166–32178.
21. Scheiner, S. Dissection of the Origin of π-Holes and the Noncovalent Bonds in Which They Engage. *J. Phys. Chem. A* **2021**, *125*, 6514–6528.
22. Kumar, M.; Balaji, P. V. CH···π Interactions in Proteins: Prevalence, Pattern of Occurrence, Residue Propensities, Location, and Contribution to Protein Stability. *J. Mol. Model.* **2014**, *20*, 1–14.
23. Wang, D.X.; Wang, M.X. Exploring Anion–π Interactions and Their Applications in Supramolecular Chemistry. *Acc. Chem. Res.* **2020**, *53*, 1364–1380.
24. Kozelka, J. Lone Pair···π Interactions in Biological Systems: Occurrence, Function, and Physical Origin. *Eur. Biophys. J.* **2017**, *46*, 729–737.
25. Das, P.; Islam, S.; Seth, S.K. Structural Elucidation and Interpretation of 2D–3D Supramolecular Assemblies Featuring Lone-Pair···π Interaction in Two Cu (II)–PDA Complexes: Experimental and Computational Assessment. *J. Mol. Struct.* **2024**, *1308*, 138088.
26. Rather, I.A.; Wagay, S.A.; Ali, R. Emergence of Anion-π Interactions: The Land of Opportunity in Supramolecular Chemistry and Beyond. *Coord. Chem. Rev.* **2020**, *415*, 213327.
27. Liu, M.; Wei, Y.; Ou, Q.; Yu, P.; Wang, G.; Duan, Y.; Geng, H.; Peng, Q.; Shuai, Z.; Liao, Y. Molecular Design Strategy for Simultaneously Strong Luminescence and High Mobility: Multichannel CH-π Interaction. *J. Phys. Chem. Lett.* **2021**, *12*, 938–946.
28. Houser, J.; Kozmon, S.; Mishra, D.; Hammerová, Z.; Wimmerová, M.; Koča, J. The CH–π Interaction in Protein–Carbohydrate Binding: Bioinformatics and In Vitro Quantification. *Chem.–Eur. J.* **2020**, *26*, 10769–10780.
29. Nagahama, S.; Inoue, K.; Sada, K.; Miyata, M.; Matsumoto, A. Two-Dimensional Hydrogen Bond Networks Supported by CH/π Interaction Leading to a Molecular Packing Appropriate for Topochemical Polymerization of 1,3-Diene Monomers. *Cryst. Growth Des.* **2003**, *3*, 247–256.
30. Desiraju, G. R.; Steiner, T. *The Weak Hydrogen Bond: In Structural Chemistry and Biology*; Oxford University Press: Oxford, UK, 2001.
31. Wheeler, S.E. Local Nature of Substituent Effects in Stacking Interactions. *J. Am. Chem. Soc.* **2011**, *133*, 10262-10274.
32. Thakuria, R.; Nath, N.K.; Saha, B.K. The Nature and Applications of π–π Interactions: A Perspective. *Cryst. Growth Des.* **2019**, *19*, 523-528.
33. Haque, A.; Alenezi, K.M.; Khan, M.S.; Wong, W.Y.; Raithby, P.R. Non-Covalent Interactions (NCIs) in π-Conjugated Functional Materials: Advances and Perspectives. *Chem. Soc. Rev.* **2023**, *52*, 454-472.
34. Jin, M.Y.; Zhen, Q.; Xiao, D.; Tao, G.; Xing, X.; Yu, P.; Xu, C. Engineered Non-Covalent π Interactions as Key Elements for Chiral Recognition. *Nat. Commun.* **2022**, *13*, 3276.
35. Koshevoy, I.O.; Krause, M.; Klein, A. Non-Covalent Intramolecular Interactions through Ligand-Design Promoting Efficient Photoluminescence from Transition Metal Complexes. *Coord. Chem. Rev.* **2020**, *405*, 213094.
36. Aitipamula, S.; Banerjee, R.; Bansal, A.K.; Biradha, K.; Cheney, M.L.; Choudhury, A.R.; Desiraju, G.R.; Dikundwar, A.G.; Dubey, R.; Duggirala, N.; et al. Polymorphs, Salts, and Cocrystals: What's in a Name? Cryst. Growth Des. 2012, 12, 2147–2152.
37. Chettri, A.; Subba, A.; Singh, G.P.; Bag, P.P. Pharmaceutical Co-Crystals: A Green Way to Enhance Drug Stability and Solubility for Improved Therapeutic Efficacy. J. Pharm. Pharmacol. 2023, 76, 1–12.
38. Hegde, T.A.; Vinitha, G. Chloridocobaltate(II) Metal–Organic Cocrystal Delivering Intermolecular-Charge Transfer-Enhanced Passive Optical Limiting: A Comprehensive Study on Structure–Property Relation. Eur. Phys. J. D 2021, 75, 214.

39. Hegde, T.A.; Dutta, A.; Sabari Girisun, T.C.; Vinitha, G. A Novel Organic-Inorganic Ionic Cocrystal—Piperazine-1,4-Diium Tetrachloridocuprate(II) Dihydrate Delivering Efficient Optical Limiting. Chem. Phys. Lett. 2021, 781, 138971–138980.
40. Kargar, H.; Behjatmanesh-Ardakani, R.; Torabi, V.; Sarvian, A.; Kazemi, Z.; Chavoshpour-Natanzi, Z.; Mirkhani, V.; Sahraei, A.; Tahir, M.N.; Ashfaq, M. Novel Copper(II) and Zinc(II) Complexes of Halogenated Bidentate N, O-Donor Schiff Base Ligands: Synthesis, Characterization, Crystal Structures, DNA Binding, Molecular Docking, DFT and TD-DFT Computational Studies. *Inorg. Chim. Acta* **2021**, *514*, 120004.
41. Kargar, H.; Behjatmanesh-Ardakani, R.; Torabi, V.; Kashani, M.; Chavoshpour-Natanzi, Z.; Kazemi, Z.; Mirkhani, V.; Sahraei, A.; Tahir, M.N.; Ashfaq, M.; Munawar, K.S. Synthesis, Characterization, Crystal Structures, DFT, TD-DFT, Molecular Docking and DNA Binding Studies of Novel Copper(II) and Zinc(II) Complexes Bearing Halogenated Bidentate N, O-Donor Schiff Base Ligands. *Polyhedron* **2021**, *195*, 114988.
42. Ay, B.; Yildiz, E.; Enomoto, M.; Okazawa, A.; Kojima, N. Crystal Structures, Gas Storage and Magnetic Properties of Lanthanide-Organic Frameworks Built Up from Dicarboxylates, $[Ln_2(2,5\text{-}pydc)_2(2,5\text{-}pipdc)(H_2O)_2]_n$ (Ln = Ce, Pr, Eu) and $(H_2pip)_n$ $[Ln_2(2,6\text{-}pydc)_4(H_2O)_2]_n$ (Ln = Ce, Pr, Eu, Sm). *Polyhedron* **2022**, *226*, 116110.
43. Shahraki, S.; Shiri, F.; Majd, M.H.; Razmara, Z. Comparative Study on the Anticancer Activities and Binding Properties of a Hetero Metal Binuclear Complex $[Co(dipic)_2Ni(OH_2)_5]\cdot 2H_2O$ (dipic = Dipicolinate) with Two Carrier Proteins. *J. Pharm. Biomed. Anal.* **2017**, *145*, 273-282.
44. Abd El-Halim, H.F.; Mohamed, G.G. Synthesis, Spectroscopic, Thermal Analyses, Biological Activity and Molecular Docking Studies on Mixed Ligand Complexes Derived from Schiff Base Ligands and 2, 6-Pyridine Dicarboxylic Acid. *Appl. Organomet. Chem.* **2018**, *32*, e4176.
45. Murinzi, T.W.; Hosten, E.; Watkins, G.M. Synthesis and Characterization of a Cobalt-2,6-Pyridinedicarboxylate MOF with Potential Application in Electrochemical Sensing. *Polyhedron* **2017**, *137*, 188-196.
46. Ma, C.; Li, J.; Zhang, R.; Wang, D. Syntheses and Characterization of Triorganotin Complexes: X-ray Crystallographic Study of Triorganotin Pyridinedicarboxylates with Trinuclear, 1D Polymeric Chain and 2D Network Structures. *J. Organomet. Chem.* **2006**, *691*, 1713-1721.
47. Diop, T.; Ndioléne, A.; Diop, M.B.; Boye, M.S.; van der Lee, A.; Dumitru, F.; Khadir Diop, C.A.; Sidibé, M. Synthesis, Spectral (FT-IR, ^1H, ^{13}C) Studies, and Crystal Structure of $[(2,6\text{-}CO_2)_2C_5H_3NSnBu_2(H_2O)]_2 \bullet CHCl_3$. *Z. Naturforsch. B* **2021**, *76*, 127-132.
48. Dutta, D.; Sharma, P.; Gomila, R.M.; Frontera, A.; Barcelo-Oliver, M.; Verma, A.K.; Baishya, T.; Bhattacharyya, M.K. Supramolecular Assemblies Involving Unconventional Non-Covalent Contacts in Pyrazole-Based Coordination Compounds of Co(II) and Cu(II) Pyridinedicarboxylates: Antiproliferative Evaluation and Theoretical Studies. *Polyhedron* **2022**, *224*, 116025.
49. Jin, S.W.; Huang, Y.; Wang, D.Q.; Fang, H.; Wang, T.; Fu, P.; Ding, L. Non-Covalently Bonded 2D–3D Metal–Organic Frameworks from the Reactions of Cd(II) and Zn(II) with 3,5-Dimethylpyrazole and Carboxylate Ligands. *Polyhedron* **2013**, *60*, 10-22.
50. Jin, S.W.; Lin, Z.H.; Zhou, Y.; Wang, D.Q.; Chen, G.Q.; Ji, Z.Y.; Huang, T. S. Syntheses, Characterization and Crystal Structures of Eight Cd(II) Carboxylates Containing 3,5-Dimethylpyrazole. *Polyhedron* **2014**, *74*, 79-92.
51. Ding, C.; Xia, M.; Wang, F.; Lei, W.; Ni, Y. The Sensitive Detection and Mechanism of Fe-3,5-Dimethyl Pyrazole Fluorescent Sensor to Diethylenetriamine Pentamethylene Phosphonic Acid: Experimental Study and Quantum Chemical Calculation. *Spectrochim. Acta A Mol. Biomol. Spectrosc.* **2022**, *281*, 121623.
52. Sarma, P.; Sharma, P.; Frontera, A.; Barcelo-Oliver, M.; Verma, A.K.; Barthakur, T.; Bhattacharyya, M.K. Unconventional π-Hole and Semi-Coordination Regium Bonding Interactions Directed Supramolecular Assemblies in Pyridinedicarboxylato Bridged Polymeric Cu(II) Compounds: Antiproliferative Evaluation and Theoretical Studies. *Inorg. Chim. Acta* **2021**, *525*, 120461.
53. Aljuhani, E.; Aljohani, M.M.; Alsoliemy, A.; Shah, R.; Abumelha, H.M.; Saad, F.A.; Hossan, A.; Al-Ahmed, Z.A.; Alharbi, A.; El-Metwaly, N.M. Synthesis and Characterization of Cu(II)-Pyrazole Complexes for Possible Anticancer Agents; Conformational Studies as well as Compatible In-Silico and In-Vitro Assays. *Heliyon* **2021**, *7*.
54. Bouroumane, N.; El Kodadi, M.; Touzani, R.; El Boutaybi, M.; Oussaid, A.; Hammouti, B.; Nandiyanto, A.B.D. New Pyrazole-Based Ligands: Synthesis, Characterization, and Catalytic Activity of Their Copper Complexes. *Arab. J. Sci. Eng.* **2022**, *47*, 269-279.

55. Santra, A.; Mondal, G.; Acharjya, M.; Bera, P.; Panja, A.; Mandal, T.K.; Mitra, P.; Bera, P. Catechol Oxidase Mimetic Activity of Copper(I) Complexes of 3,5-Dimethyl Pyrazole Derivatives: Coordination Behavior, X-ray Crystallography and Electrochemical Study. *Polyhedron* **2016**, *113*, 5-15.
56. Devkule, S.S.; More, M.S.; Chavan, S.S. Synthesis, Characterization, Luminescence and Catalytic Properties of Copper(I) Complexes with N-(2-Pyridylmethylene)-1,5-Dimethyl-2-Pyrazole-3-(2H)-one and Triphenylphosphine as Ligands. *Inorg. Chim. Acta* **2017**, *455*, 183-189.
57. Titov, A.A.; Filippov, O.A.; Smol'yakov, A.F.; Averin, A.A.; Shubina, E.S. Copper(I) Complex with BINAP and 3,5-Dimethylpyrazole: Synthesis and Photoluminescent Properties. *Mendeleev Commun.* **2019**, *29*, 570-572.
58. Turecka, K.; Chylewska, A.; Rychłowski, M.; Zakrzewska, J.; Waleron, K. Antibacterial Activity of Co(III) Complexes with Diamine Chelate Ligands Against a Broad Spectrum of Bacteria with a DNA Interaction Mechanism. *Pharmaceutics* **2021**, *13*, 946.
59. Turecka, K.; Chylewska, A.; Rychłowski, M.; Zakrzewska, J.; Waleron, K. Antibacterial Activity of Co(III) Complexes with Diamine Chelate Ligands Against a Broad Spectrum of Bacteria with a DNA Interaction Mechanism. *Pharmaceutics* **2021**, *13*, 946.
60. Condé, C.A.; De Almeida, M.V.; Da Silva, G.D.S.; Sodré, M.B.P.D.A.; Rodrigues, J.C.F.; Navarro, M. Synthesis, Characterization and Antileishmanial Activity of Copper(II) and Zinc(II) Complexes with Diamine Ligands. *Transition Met. Chem.* **2022**, *47*, 147-156.
61. Rajeshwari, K.; Anantha Lakshmi, P.V.; Archana, J.; Sumakanth, M. Ternary Cobalt(II), Nickel(II), and Copper(II) Complexes Containing Metformin and Ethylenediamine: Synthesis, Characterization, Thermal, In Vitro DNA Binding, In Silico Molecular Docking, and In Vivo Antihyperglycemic Studies. *Appl. Organomet. Chem.* **2021**, *35*, e6100.
62. Boudiombo, J.S.B.; Su, H.; Ravenscroft, N.; Bourne, S.A.; Nassimbeni, L.R. Selective Enclathration of Xylenols: Synergistic Effects of Mixed Hosts. *CrystEngComm* **2020**, *22*, 7389-7398.
63. Morohashi, N.; Hattori, T. Selective Guest Inclusion by Crystals of Calixarenes: Potential for Application as Separation Materials. *J. Incl. Phenom. Macrocycl. Chem.* **2018**, *90*, 261-277.
64. Colorado-Peralta, R.; Rivera-Villanueva, J.M.; Mora-Hernández, J.M.; Morales-Morales, D.; Alfonso-Herrera, L.Á. An Overview of the Role of Supramolecular Interactions in Gas Storage Using MOFs. *Polyhedron* **2022**, *224*, 115995.
65. Das, R.K.; Aijaz, A.; Sharma, M.K.; Lama, P.; Bharadwaj, P.K. Direct Crystallographic Observation of Catalytic Reactions Inside the Pores of a Flexible Coordination Polymer. *Chem. - Eur. J.* **2012**, *18*, 6866-6872.
66. Baishya, T.; Gomila, R.M.; Frontera, A.; Barcelo-Oliver, M.; Verma, A.K.; Bhattacharyya, M.K. Enclathration of Mn(II)$(H_2O)_6$ Guests and Unusual Cu···O Bonding Contacts in Supramolecular Assemblies of Mn(II) Co-Crystal Hydrate and Cu(II) Pyridinedicarboxylate: Antiproliferative Evaluation and Theoretical Studies. *Polyhedron* **2023**, *230*, 116243.
67. Bhattacharyya, M.K.; Banik, S.; Baishya, T.; Sharma, P.; Dutta, K.K.; Gomila, R.M.; Barcelo-Oliver, M.; Frontera, A. Fascinating Inclusion of Metal–Organic Complex Moieties in Dinuclear Mn(II) and Zn(II) Compounds Involving Pyridinedicarboxylates and Phenanthroline: Experimental and Theoretical Studies. *Polyhedron* **2024**, *254*, 116947.
68. Das, A.; Sharma, P.; Gomila, R.M.; Frontera, A.; Verma, A.K.; Sarma, B.; Bhattacharyya, M.K. Synthesis, Structural Topologies and Anticancer Evaluation of Phenanthroline-Based 2,6-Pyridinedicarboxylato Cu(II) and Ni(II) Compounds. *Polyhedron* **2022**, *213*, 115632.
69. Dutta, D.; Sharma, P.; Gomila, R.M.; Frontera, A.; Barcelo-Oliver, M.; Verma, A.K.; Gogoi, M.; Bhattacharyya, M.K. Solvent Driven Structural Topologies Involving Unconventional OH (Methanol)···π Contact and Anti-Cooperative HB···Anion-π···HB Assemblies with Unusual Enclathration of Dual Guest $(H_2O)_4$ Cores in Mn(II) and Ni(II) Coordination Compounds: Antiproliferative Evaluation and Theoretical Studies. *Polyhedron* **2021**, *210*, 115503.
70. Das, A.; Choudhury, S.R.; Estarellas, C.; Dey, B.; Frontera, A.; Hemming, J.; Helliwell, M.; Gamez, P.; Mukhopadhyay, S. Supramolecular Assemblies Involving Anion–π and Lone Pair–π Interactions: Experimental Observation and Theoretical Analysis. *CrystEngComm* **2011**, *13*, 4519.
71. Basak, T.; Frontera, A.; Chattopadhyay, S. Synthesis and Characterization of a Mononuclear Zinc(II) Schiff Base Complex: On the Importance of C–H···π Interactions. *RSC Adv.* **2021**, *11*, 30148-30155.

72. Gogoi, A.; Das, A.; Frontera, A.; Verma, A.K.; Bhattacharyya, M.K. Energetically Significant Unconventional π-π Contacts Involving Fumarate in a Novel Coordination Polymer of Zn(II): In-Vitro Anticancer Evaluation and Theoretical Studies. *Inorg. Chim. Acta* **2019**, *493*, 1.
73. Kokina, T.E.; Glinskaya, L.A.; Tkachev, A.V.; Plyusnin, V.F.; Tsoy, Y.V.; Bagryanskaya, I.Y.; Vasilyev, E.S.; Piryazev, D.A.; Sheludyakova, L.A.; Larionov, S.V. Chiral Zinc(II) and Cadmium(II) Complexes with a Dihydrophenanthroline Ligand Bearing (–)-α-Pinene Fragments: Synthesis, Crystal Structures and Photophysical Properties. *Polyhedron* **2016**, *117*, 437.
74. Das, S.; Bharadwaj, P.K. Self-Assembly of a Luminescent Zinc(II) Complex: A Supramolecular Host–Guest Fluorescence Signaling System for Selective Nitrobenzene Inclusion. *Inorg. Chem.* **2006**, *45*, 5257.
75. Chakravorty, S.; Platts, J.A.; Das, B.K. Novel C–H···C Contacts Involving 3,5-Dimethylpyrazole Ligands in a Tetracoordinate Co(II) Complex. *Dalton Trans.* **2011**, *40*, 11605.
76. Mahapatra, T.S.; Bauzá, A.; Dutta, D.; Mishra, S.; Frontera, A.; Ray, D. Carboxylate Coordination Assisted Aggregation for Quasi-Tetrahedral and Partial-Dicubane [Cu_4] Coordination Clusters. *Chem. Select.* **2016**, *1*, 64.
77. Orhan, O.; Çolak, A.T.; Emen, F.M.; Kismali, G.; Meral, O.; Sel, T.; Çilgi, G.K.; Taş, M. Syntheses of Crystal Structures and In Vitro Cytotoxic Activities of New Copper(II) Complexes of Pyridine-2,6-Dicarboxylate. *J. Coord. Chem.* **2015**, *68*, 4003.
78. Manna, S.C.; Mistri, S.; Jana, A.D. A Rare Supramolecular Assembly Involving Ion Pairs of Coordination Complexes with a Host–Guest Relationship: Synthesis, Crystal Structure, Photoluminescence and Thermal Study. *CrystEngComm* **2012**, *14*, 7415.
79. Debnath, P.; Singh, K.S.; Singh, K.K.; Singh, S.S.; Sieroń, L.; Maniukiewicz, W. Di-Butyltin(IV) Complexes with Azo-Carboxylates: Synthesis, Characterization, Crystal Structures and Their Anti-Diabetic Assay. *New J. Chem.* **2020**, *44*, 5862.
80. Hashemi, M.; Mohandes, F.; Ahmadian-Fard-Fini, S.; Sobhani, A.; Shabani-Armaki, N.; Salavati-Niasari, M. Solvent-Free Preparation of Copper Ferrite Microspheres Composed of Nanorods Using a New Coordination Compound as Precursor. *J. Mater. Sci.: Mater. Electron.* **2017**, *28*, 11682.
81. Nakamoto, K. *Infrared and Raman Spectra of Inorganic and Coordination Compounds*; Wiley: New York, 1986; p 203.
82. Li, J.; Xing, Y.H.; Zhao, H.Y.; Li, Z.P.; Wang, C.G.; Zeng, X.Q.; Ge, M.F.; Niu, S.Y. Constructions of a Set of Hydrogen-Bonded Supramolecules from Reactions of Transition Metals with 3,5-Dimethylpyrazole and Different Dicarboxylate Ligands. *Inorg. Chim. Acta* **2009**, *362*, 2788.
83. Lu, Y.; Xu, W.; Hu, K.; Jin, S.; Sun, L.; Liu, B.; Wang, D. Synthesis and Structural Characterizations of Nine Non-Covalent-Bonded Zn^{2+} and Cd^{2+} Supramolecules Based on 3,5-Dimethylpyrazole and Carboxylates. *Polyhedron* **2019**, *159*, 408.
84. Titi, A.; Shiga, T.; Oshio, H.; Touzani, R.; Hammouti, B.; Mouslim, M.; Warad, I. Synthesis of Novel [$Cl_2Co_4L_6$] Cluster Using 1-Hydroxymethyl-3,5-Dimethylpyrazole (LH) Ligand: Crystal Structure, Spectral, Thermal, Hirschfeld Surface Analysis and Catalytic Oxidation Evaluation. *J. Mol. Struct.* **2020**, *1199*, 126995.
85. Direm, A.; Tursun, M.; Parlak, C.; Benali-Cherif, N. Trans-Dichlorotetrakis(1H-Pyrazole-κN_2) Copper(II): Synthesis, Crystal Structure, Hydrogen Bonding Graph-Sets, Vibrational and DFT Studies. *J. Mol. Struct.* **2015**, *1093*, 208.
86. Mautner, F.A.; Scherzer, M.; Berger, C.; Fischer, R.C.; Vicente, R.; Massoud, S.S. Synthesis and Characterization of Five New Thiocyanato- and Cyanato-Metal(II) Complexes with 4-Azidopyridine as Co-Ligand. *Polyhedron* **2015**, *85*, 20-26.
87. Figgis, B.N.; Hitchman, M.A. *Ligand Field Theory and Its Applications*; Wiley-VCH: New York, 2000; p 209.
88. Sharma, P.; Sarma, P.; Frontera, A.; Hussain, S.; Verma, A.K.; Bhattacharyya, M.K. Energetically Significant Anti-Parallel π-Stacking and Unconventional Anion-π Interactions in Phenanthroline-Based Ni(II) and Cu(II) Coordination Compounds: Antiproliferative Evaluation and Theoretical Studies. *Inorganica Chimica Acta* **2021**, *516*, 120082.
89. Dutta, D.; Nashre-ul-Islam, S.M.; Saha, U.; Frontera, A.; Bhattacharyya, M.K. Cu(II) and Co(II) Coordination Solids Involving Unconventional Parallel Nitrile (π)–Nitrile (π) and Energetically Significant Cooperative Hydrogen Bonding Interactions: Experimental and Theoretical Studies. *J. Mol. Struct.* **2019**, *1195*, 733-743.

 doi:10.20944/preprints202408.1099.v1

90. Araújo, E.L.; Barbosa, H.F.G.; Dockal, E.R.; Cavalheiro, E.T.G. Synthesis, Characterization and Biological Activity of Cu(II), Ni(II) and Zn(II) Complexes of Biopolymeric Schiff Bases of Salicylaldehydes and Chitosan. *Int. J. Biol. Macromol.* **2017**, *95*, 168.
91. Ekennia, A.C.; Onwudiwe, D.C.; Osowole, A.A.; Olasunkanmi, L.O.; Ebenso, E.E. Synthesis, Biological, and Quantum Chemical Studies of Zn(II) and Ni(II) Mixed-Ligand Complexes Derived from N,N-Disubstituted Dithiocarbamate and Benzoic Acid. *J. Chem.* **2016**, *55*, 1.
92. Bordbar, M.; Tabatabaee, M.; Alizadeh-Nouqi, M.; Mehri-Lighvan, Z.; Khavasi, H.R.; YeganehFaal, A.; Fallahian, F.; Dolati, M. Synthesis, Characterization, Cytotoxic Activity and DNA-Binding Studies of Cobalt(II) Mixed-Ligand Complex Containing Pyridine-2,6-Dicarboxylate Ion and 2-Aminopyrimidine. *J. Iranian Chem. Soc.* **2016**, *13*, 1125-1132.
93. Chakravorty, S.; Platts, J.A.; Das, B.K. Novel C–H···C Contacts Involving 3,5-Dimethylpyrazole Ligands in a Tetracoordinate Co(II) Complex. *Dalton Trans.* **2011**, *40*, 11605.
94. Ghosh, M.; Majee, A.; Nethaji, M.; Chattopadhyay, T. Syntheses and Characterization of trans-[$NiL_2(NCS)_2$][L = 2-(Aminomethyl) Pyridine], trans-[$NiL_2'(NSC)_2$][L′ = 2-(2-Aminoethyl) Pyridine] and trans-[$NiL_2''(NSC)_2$][L″ = 2-(2-Methylaminoethyl) Pyridine] Complexes: X-Ray Single Crystal Structure of trans-[$NiL_2'(NSC)_2$][L′ = 2-(2-Aminoethyl) Pyridine]. *Inorganica Chimica Acta* **2009**, *362*, 2052-2055.
95. Bhattacharyya, M.K.; Gogoi, A.; Chetry, S.; Dutta, D.; Verma, A.K.; Sarma, B.; Franconetti, A.; Frontera, A. Antiproliferative Evaluation and Supramolecular Association in Mn(II) and Zn(II) Bipyridine Complexes: Combined Experimental and Theoretical Studies. *J. Inorg. Biochem.* **2019**, *200*, 110803.
96. Osypiuk, D.; Cristóvão, B.; Bartyzel, A. New Coordination Compounds of Cu(II) with Schiff Base Ligands—Crystal Structure, Thermal, and Spectral Investigations. *Crystals* **2020**, *10*, 1004.
97. El-Sonbati, A.Z.; Diab, M.A.; Morgan, S.M.; Abou-Dobara, M.I.; El-Ghettany, A.A. Synthesis, Characterization, Theoretical and Molecular Docking Studies of Mixed-Ligand Complexes of Cu(II), Ni(II), Co(II), Mn(II), Cr(III), UO_2(II) and Cd(II). *J. Mol. Struct.* **2020**, *1200*, 127065.
98. Yang, L.; Wu, B.; Zhang, T.; Liu, Z.; Zhang, J. Preparation, Crystal Structure, Thermal Decomposition, and Explosive Properties of [$Cd(en)(N_3)_2]_n$. *Propellants, Explosives, Pyrotechnics* **2010**, *35*, 521-528.
99. Etaiw, S.E.H.; El-Bendary, M.M.; Abdelazim, H. Synthesis, Characterization, and Biological Activity of Cd(II) and Mn(II) Coordination Polymers Based on Pyridine-2,6-Dicarboxylic Acid. *Russian J. Coord. Chem.* **2017**, *43*, 320-330.
100. Sarma, P.; Sharma, P.; Gomila, R.M.; Frontera, A.; Barcelo-Oliver, M.; Verma, A.K.; Baruwa, B.; Bhattacharyya, M.K. Charge Assisted Hydrogen Bonded Assemblies and Unconventional O···O Dichalcogen Bonding Interactions in Pyrazole-Based Isostructural Ni(II) and Mn(II) Compounds Involving Anthraquinone Disulfonate: Antiproliferative Evaluation and Theoretical Studies. *J. Mol. Struct.* **2022**, *1250*, 131883.
101. da Silva, P.B.; Terra, P.H.; Frem, R.C.; Netto, A.V.; Mauro, A.E. Synthesis, Characterization, and Investigation of the Thermal Behavior of Cu(II) Pyrazolyl Complexes. *J. Therm. Anal. Calorim.* **2011**, *106*, 495-499.
102. Liu, M.S.; Yu, Q.Y.; Cai, Y.P.; Su, C.Y.; Lin, X.M.; Zhou, X.X.; Cai, J.W. One-, Two-, and Three-Dimensional Lanthanide Complexes Constructed from Pyridine-2,6-Dicarboxylic Acid and Oxalic Acid Ligands. *Crystal Growth Des.* **2008**, *8*, 4083-4091.
103. Das, A.; Sharma, P.; Gomila, R.M.; Frontera, A.; Verma, A.K.; Sarma, B.; Bhattacharyya, M.K. Synthesis, Structural Topologies and Anticancer Evaluation of Phenanthroline-Based 2,6-Pyridinedicarboxylato Cu(II) and Ni(II) Compounds. *Polyhedron* **2022**, *213*, 115632.
104. SADABS. Version 2.05; Bruker AXS: Madison, USA, 1999.
105. Sheldrick, G.M. Crystal Structure Refinement with SHELXL. *Acta Crystallogr., Sect. A: Found. Crystallogr.* **2008**, *64*, 112.
106. Farrugia, L.J. WinGX and ORTEP for Windows: An Update. *J. Appl. Crystallogr.* **1999**, *32*, 837.
107. Brandenburg, K. Diamond 3.1f; Crystal Impact GbR: Bonn, Germany, 2008.
108. Ahlrichs, R.; Bar, M.; Hacer, M.; Horn, H.; Kömel, C. Electronic Structure Calculations on Workstation Computers: The Program System TURBOMOLE. *Chem. Phys. Lett.* **1989**, *162*, 165.
109. Adamo, C.; Barone, V. Toward Reliable Density Functional Methods Without Adjustable Parameters: The PBE0 Model. *J. Chem. Phys.* **1999**, *110*, 6158-6170.

 doi:10.20944/preprints202408.1099.v1

110. Grimme, S.; Antony, J.; Ehrlich, S.; Krieg, H. A Consistent and Accurate Ab Initio Parametrization of Density Functional Dispersion Correction (DFT-D) for the 94 Elements H–Pu. *J. Chem. Phys.* **2010**, *132*, 154104.
111. Weigend, F. Accurate Coulomb-Fitting Basis Sets for H to Rn. *Phys. Chem. Chem. Phys.* **2006**, *8*, 1057.
112. Bader, R.F.W. Atoms in Molecules. *Chem. Rev.* **1991**, *91*, 893.
113. Contreras-Garcia, J.; Johnson, E.R.; Keinan, S.; Chaudret, R.; Piquemal, J.P.; Beratan, D.N.; Yang, W. NCIPLOT: A Program for Plotting Non-Covalent Interaction Regions. *J. Chem. Theory Comput.* **2011**, *7*, 625.
114. Lu, T.; Chen, F. Multiwfn: A Multifunctional Wavefunction Analyzer. *J. Comput. Chem.* **2012**, *33*, 580.
115. Humphrey, W.; Dalke, A.; Schulten, K. VMD: Visual Molecular Dynamics. *J. Mol. Graph.* **1996**, *14*, 33.
116. Espinosa, E.; Molins, E.; Lecomte, C. Hydrogen Bond Strengths Revealed by Topological Analyses of Experimentally Observed Electron Densities. *Chem. Phys. Lett.* **1998**, *285*, 170.